Maturation, developmental site, and pathology dictate murine neutrophil function

John B. G. Mackey[1,3*], Amanda J. McFarlane[1], Thomas Jamieson[1], Rene Jackstadt[1,4], Ximena L. Raffo-Iraolagoitia[1], Judith Secklehner[1,3], Xabier Cortes-Lavaud[1], Frédéric Fercoq[1], William Clarke[1], Ann Hedley[1], Kathryn Gilroy[1], Sergio Lilla[1], Juho Vuononvirta[3,5], Gerard J. Graham[6], Katia De Filippo[3], Daniel J. Murphy[1,2], Colin W. Steele[1,2], Jim C. Norman[1,2], Thomas G. Bird[1,7], Derek A. Mann[8], Jennifer P. Morton[1,2], Sara Zanivan[1,2], Owen J. Sansom[1,2], Leo M. Carlin[1,2,3*]

[1]Cancer Research UK Beatson Institute, Garscube Estate, Switchback Road, Glasgow, G61 1BD, UK

[2]Institute of Cancer Sciences, University of Glasgow, Garscube Estate, Switchback Road, Glasgow, G61 1BD, UK

[3]Inflammation, Repair & Development, Imperial College London, London, UK

[4]Current address: HI-STEM, Heidelberg, Germany

[5]Current address: William Harvey Research Institute, London, UK.

[6]Chemokine Research Group, University of Glasgow, Glasgow, UK.

[7]MRC Centre for Inflammation Research, The Queen's Medical Research Institute, University of Edinburgh, EH16 4TJ, UK

[8]Newcastle Fibrosis Research Group, Bioscience Institute, Faculty of Medical Sciences, Newcastle University, Newcastle-upon-Tyne, UK

[*]Correspondence

Leo M. Carlin, Cancer Research UK Beatson Institute, Garscube Estate, Switchback Road, Glasgow, United Kingdom, G61 1BD

Email: leo.carlin@glasgow.ac.uk

Abstract

Neutrophils have been implicated in poor outcomes in cancer and severe inflammation. We found that neutrophils expressing intermediate levels of Ly6G (Ly6G^{Int}) were present in mouse cancer models and more abundant in those with high rates of spontaneous metastasis. Maturation, age, tissue localization and functional capacity all drive neutrophil heterogeneity. Recent studies have proposed various markers to distinguish between these heterogeneous sub-populations; however, these markers are limited to specific models of inflammation and cancer. Here, we identify and define Ly6G expression level as a robust and reliable marker to distinguish neutrophils at different stages of maturation. Ly6G^{Int} neutrophils were bona fide 'immature neutrophils' with reduced immune regulatory and adhesion capacity. Whereas the bone marrow is a more recognised site of granulopoiesis, the spleen also produces neutrophils in homeostasis and cancer. Strikingly, neutrophils matured faster in the spleen than in the bone marrow with unique transcriptional profiles. We propose that developmental origin is critical in neutrophil identity and postulate that neutrophils that develop in the spleen supplement the bone marrow by providing an intermediate more mature reserve before emergency haematopoiesis.

Introduction

Neutrophils comprise a complex heterogeneous myeloid subset that becomes increasingly diverse with disease progression[1]. Neutrophil heterogeneity has been proposed to be influenced by a multitude of factors including maturation stage and age[2], tissue localization[3] and functional capacity[4]. Importantly, there is significant overlap between these heterogeneous neutrophil phenotypes. For example, immature neutrophils in the spleen are less motile, respond differently to bacterial infection, and localize differently when compared to mature splenic neutrophils[5, 6].

Stages of neutrophil maturation can be characterised by distinct morphological and transcriptional phenotypes that are closely associated with functional capacity[7, 8, 9]. In disease, immature neutrophils can be prematurely released from the bone marrow (BM) and have been identified in a range of pathologies including cancer[4, 10], sepsis[11], and more recently severe SARS-CoV-2 infection[12], where they have been proposed as biomarkers for disease progression and outcome. Differences in the functional capacity of immature and mature neutrophils have been proposed in mice and humans, including NETosis[13], metabolism[14], chemotaxis and oxidative capacity[10]. However, diversity in the methods used to identify immature neutrophils combined with the range of models investigated makes comprehensive interpretation of results in this area challenging[15]. Recent evidence for tissue specific transcriptional phenotypes[3] and disease induced transcriptional and developmental alterations[8, 16] further add to this complexity.

The functional influence and disease importance of neutrophil development and maturation remain poorly understood. Here, we provide comprehensive evidence that the maturation landscape and developmental niche are crucial to our understanding of the role of neutrophils in disease. Neutrophils expressing intermediate levels of (Ly6G^{Int}) were identified in several mouse cancer models. These were demonstrably less mature than their Ly6G-high (Ly6G^{Hi}) counterparts with specific transcriptional profiles and reduced functional capacity. Identification of maturation status based on Ly6G expression was accurate across naïve, acute inflammatory and cancer models where in the latter Ly6G^{Int} neutrophil abundance associated with metastatic potential. Furthermore, we identified that the site of neutrophil development influences their maturation and phenotype. Although the BM is a more recognised site of granulopoiesis, the spleen also produces neutrophils in homeostasis and cancer. We found that immature splenic-derived

66 neutrophils underwent a more rapid maturation with altered transcriptomic, phenotypic, and functional
67 capacity in a steady state and in cancer models compared to their BM-derived counterparts. We propose
68 that this indicates a distinct role for splenic-derived neutrophils in innate immunity as a secondary source of
69 more functionally competent / active neutrophils that supplement circulating and Ly6G^{Hi} BM reserve cells.
70

71 **Results**

72 **Ly6G^{Int} neutrophil abundance associates with metastatic potential in mouse cancer models**

73 We studied the neutrophils from a panel of preclinical mouse cancer models. In homeostasis, peripheral
74 blood neutrophils are almost exclusively Ly6G^{Hi}, with neutrophils expressing intermediate Ly6G levels
75 (Ly6G^{Int}) restricted to the BM (**Fig. 1a, full gating strategy Extended Data Fig. 1a**). Interestingly, we observed
76 shifts in Ly6G expression in several of the cancer models studied. Ly6G^{Int} neutrophils in the peripheral blood
77 and tissues of metastatic colorectal cancer (CRC) *Villin-cre*^{ER}; *Kras*$^{G12D/+}$; *Trp53*$^{fl/fl}$; *Rosa26*$^{N1icd/+}$ (KPN) mice[17]
78 increased with tumour progression, reaching significance at clinical endpoint compared to day 30 post-
79 tamoxifen induction controls (**Fig. 1b-d**). In contrast, Ly6G^{Int} neutrophils were not increased in the poorly
80 metastatic models tested. These were lung adeno-*Cre* driven *KRas*$^{G12D/+}$; *Rosa26*$^{lsl\text{-}Myc/lsl\text{-}Myc}$ (KM)[18] lung
81 adenocarcinoma bearing mice induced at a virus titre where metastases do not form before endpoint (**Fig.
82 1e-g**), and Diethylnitrosamine-American lifestyle induced obesity syndrome (DEN/ALIOS) driven
83 hepatocellular carcinoma bearing mice (**Fig. 1h-j**). To determine whether Ly6G^{Int} neutrophils associate with
84 metastatic potential in the same cancer type, we compared poorly-metastatic *Kras*$^{G12D/+}$; *Trp53*$^{fl/+}$; *Pdx1-Cre*
85 (KP^{fl}C) and highly-metastatic *Kras*$^{G12D/+}$; *Trp53*$^{R172H/+}$; *Pdx1-Cre* (KPC) mouse models of pancreatic ductal
86 adenocarcinoma (PDAC)[19] to age-matched wild-type (WT) and *Kras*$^{G12D/+}$; *Pdx1-Cre* (KC; where only pancreatic
87 intraepithelial neoplasia develops) controls (**Fig. 1k**). Here, KP^{fl}C and KPC mice were taken with a similarly
88 sized palpable primary tumour but prior to overt metastasis. Ly6G^{Int} neutrophils increased systemically from
89 WT to KC, KP^{fl}C and KPC respectively, correlating with the presence of lesions and metastatic potential (**Fig.
90 1l-p**). This increase was most apparent in the lung and liver of KPC mice, the two primary sites of metastasis
91 in this model (**Fig. 1o, p**). Thus, the abundance of Ly6G^{Int} neutrophils mirrored metastatic potential in a panel
92 of mouse models of cancer with different origins and drivers.

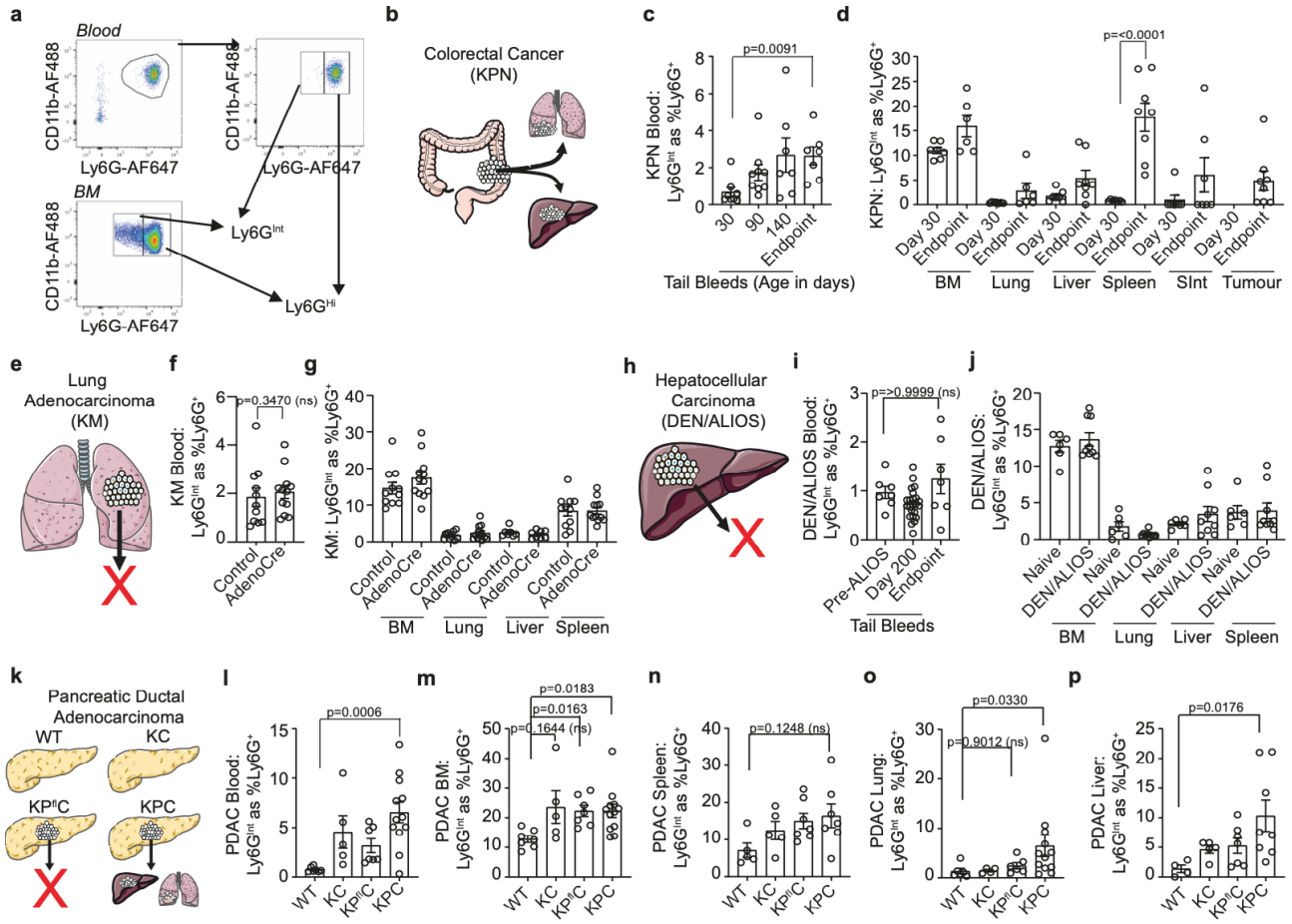

Fig 1. Ly6G^{Int} neutrophils associate with metastasis and metastatic potential. **a**, Ly6G^{Int} and Ly6G^{Hi} neutrophil populations were identified from the Ly6G^{+}CD11b^{+} population. Ly6G^{Hi} neutrophils are predominant in the peripheral blood of naïve mice and were gated. All Ly6G^{+} neutrophils not falling into the Ly6G^{Hi} population were gated as Ly6G^{Int}. **b**, Schematic for metastatic colorectal cancer mouse model, termed KPN. **c**, Quantification of Ly6G^{Int} as %Ly6G^{+} neutrophils in the peripheral blood of KPN mice. Day 30 n=8 mice; day 90 n=9 mice; day 140 n=7 mice; endpoint n=7 mice. Data were analysed by Kruskal-Wallis test with Dunn's multiple comparisons test. **d**, Quantification of Ly6G^{Int} as %Ly6G^{+} neutrophils in the tissues of KPN mice. Bone marrow (BM): day 30 n=7 mice; endpoint n=6 mice. Lung: day 30 n=7 mice; endpoint n=6 mice. Liver: day 30 n=7 mice; endpoint n=8 mice. Spleen: day 30 n=7 mice; endpoint n=8 mice. Small intestine (SInt): day 30 n=7 mice; endpoint n=8 mice. Tumour: endpoint n=8 mice. Data were analysed by 2way ANOVA with Sidak's multiple comparisons test. **e**, Schematic for non-metastatic lung adenocarcinoma mouse model, termed KM. **f**, Quantification of Ly6G^{Int} as %Ly6G^{+} neutrophils in the peripheral blood of KM mice. Control n=11 mice; AdenoCre n=12 mice. Data were analysed by Mann-Whitney test. **g**, Quantification of Ly6G^{Int} as %Ly6G^{+} neutrophils in the tissues of KM mice. BM: control n=11 mice; AdenoCre n=13 mice. Lung: control n=11 mice; AdenoCre n=12 mice. Liver: control n=7 mice; AdenoCre n=8 mice. Spleen: control n=11 mice; AdenoCre n=12 mice. Data were analysed by 2way ANOVA with Sidak's multiple comparisons test. **h**, Schematic for non-metastatic hepatocellular carcinoma mouse model, termed DEN/ALIOS. **i**, Quantification of Ly6G^{Int} as %Ly6G^{+} neutrophils in the peripheral blood of DEN/ALIOS mice. Pre-ALIOS n=7 mice; day 200 n=23 mice; endpoint n=7 mice. Data were analysed by Kruskal-Wallis test with Dunn's multiple comparisons test. **j**, Quantification of Ly6G^{Int} as %Ly6G^{+} neutrophils in the tissues of DEN/ALIOS mice. All tissues: naïve n=6 mice; DEN/ALIOS n=9 mice. Data were analysed by 2way ANOVA with Sidak's multiple comparisons test. **k**, Schematic for WT-control, KC-control, KP^{fl}C non-metastatic and KPC metastatic mouse models of pancreatic ductal adenocarcinoma. **l**, Quantification of Ly6G^{Int} as %Ly6G^{+} neutrophils in the peripheral blood of WT, KC, KP^{fl}C and KPC mice. WT n=7 mice; KC n=5 mice; KP^{fl}C n=7 mice; KPC n=12 mice. Data were analysed by Kruskal-Wallis test with Dunn's multiple comparisons test. **m**, Quantification of Ly6G^{Int} as %Ly6G^{+} neutrophils in the BM of WT, KC, KP^{fl}C and KPC mice. WT n=7 mice; KC n=5 mice; KP^{fl}C n=7 mice; KPC n=12 mice. Data were analysed by Kruskal-Wallis test with Dunn's multiple comparisons test. **n**, Quantification of Ly6G^{Int} as %Ly6G^{+} neutrophils in the spleen of WT, KC, KP^{fl}C and KPC mice. WT n=6 mice; KC n=4 mice; KP^{fl}C n=6 mice; KPC n=12 mice. Data were analysed by Kruskal-Wallis test with Dunn's multiple comparisons test. **o**, Quantification of Ly6G^{Int} as %Ly6G^{+} neutrophils in the lung of WT, KC, KP^{fl}C and KPC mice. WT n=4 mice; KC n=5 mice; KP^{fl}C n=7 mice; KPC n=8 mice. Data were analysed by Kruskal-Wallis test with Dunn's multiple comparisons test. **p**, Quantification of Ly6G^{Int} as %Ly6G^{+} neutrophils in the liver of WT, KC, KP^{fl}C and KPC mice. WT n=5 mice; KC n=5 mice; KP^{fl}C n=7 mice; KPC n=7 mice. Data were analysed by Kruskal-Wallis test with

Dunn's multiple comparisons test. Dots in Fig. 1c-d, f-g, i-j, l-p represent individual mice. Error bars in Fig. 1c-d, f, g, i, j, l-p represent mean±SEM.

Ly6G surface expression accurately identifies neutrophil maturity

Neutrophils that express intermediate levels of Ly6G are thought to be immature, but this hasn't been comprehensively tested and compared with other signifiers of maturity. Therefore, we next sought to test the use of Ly6G expression as a universal marker for neutrophil maturity. Consistent with a more immature population, Ly6G^{Int} neutrophils were: restricted to the BM in a steady state, had reduced side-scatter by flow cytometry indicative of lower granularity, had a less segmented nuclear morphology compared to Ly6G^{Hi} neutrophils, and constituted a greater percentage of the Ly6G^{+}CD11b^{+} populations in the BM and peripheral blood of CSF-3- and LPS-challenged mice (**Fig. 2a-c and Extended Data Fig. 2a, b**). Furthermore, when we cultured BM-derived Ly6G^{Int} neutrophils, they increased cell surface Ly6G and were more viable over 20 hours than their Ly6G^{Hi} counterparts (**Fig. 2d-f**). Neutrophils exit the mitotic pool during transition from the myelocyte to metamyelocyte stages of development[20, 21]. Cells that incorporated the thymidine analogue EdU during mitosis composed a greater percentage of Ly6G^{Int} compared to Ly6G^{Hi} neutrophils in the BM of PBS-control mice between 4 and 24 hours post-EdU incorporation (**Fig. 2g**). These results were replicated in G-CSF (CSF-3)-[22, 23] and LPS-challenge[24] mouse models to induce haematopoietic stress in which immature neutrophils are identified outside of their medullary niche in mice and humans.(**Fig. 2g**). In contrast to PBS controls, EdU^{+} neutrophils were identified in the peripheral blood as early as 24 hours post-EdU injection in CSF-3- and LPS-challenged mice (**Extended Data Fig. 2c**). Of these, a significantly higher percentage of Ly6G^{Int} neutrophils were EdU^{+} compared to the Ly6G^{Hi} population (**Fig. 2g**). Ki-67 staining confirmed that a proportion of BM Ly6G^{Int} neutrophils were outside of G_0, however, Ki-67 expression was drastically reduced in the BM of CSF-3- and LPS-challenged mice (**Extended Data Fig. 2d**). These data are consistent with Ly6G^{Int} neutrophils being more recently actively mitotic compared to Ly6G^{Hi} neutrophils and a shift from cell cycle regulation to quicker post-mitotic maturation and efflux from the BM in states of haematopoietic stress[16]. Transcriptomic analysis showed clear differences between Ly6G^{Int} and Ly6G^{Hi} neutrophils dependent on tissue and stimulus (**Extended Data Fig. 2e, f**).

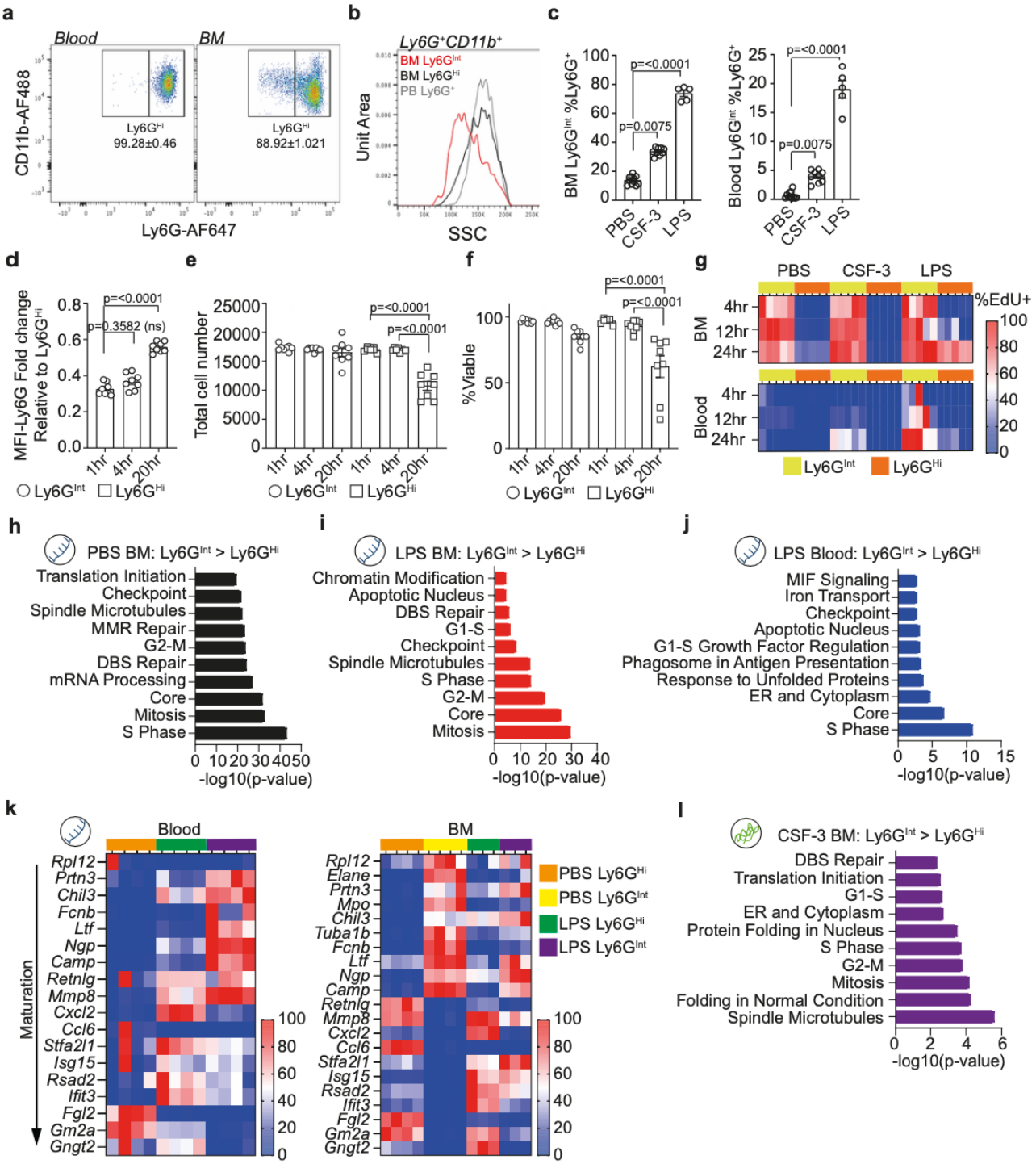

Fig. 2. Intermediate surface Ly6G expression accurately and consistently identifies neutrophil immaturity. a, Flow cytometry plot for Ly6G^{Int} and Ly6G^{Hi} neutrophils in the peripheral blood and BM of naive mice. Data are presented as mean±standard deviation. Data representative of n=5 mice. **b**, Histogram showing flow cytometric SSC profile for BM Ly6G^{Int}, BM Ly6G^{Hi} and peripheral blood Ly6G^{+} neutrophils from naïve mice. Data representative of n=5 mice. **c**, Quantification of Ly6G^{Int} as %Ly6G^{+} in the BM (left) and peripheral blood (right). PBS n=11 mice; CSF-3 n=9 mice; LPS n=5 mice. Data were analysed by Kruskal-Wallis test with Dunn's multiple comparisons test. **d**, Quantification of MFI-Ly6G fold change for Ly6G^{Int} relative to Ly6G^{Hi} neutrophils isolated from naïve mice following *ex vivo* culture. 1hr time-point n=8 mice; 4hr time-point n=8 mice; 20hr time-point n=8 mice. Data were analysed by Kruskal-Wallis test with Dunn's multiple comparisons test. **e**, Quantification of total cell no. recovered for Ly6G^{Int} and Ly6G^{Hi} neutrophils isolated from naïve mice following *ex vivo* culture. 1hr time-point n=8 mice; 4hr time-point n=8 mice; 20hr time-point n=8 mice. Data were analysed by 2way ANOVA with Tukey's multiple comparisons test. **f**, Quantification of %Viable Ly6G^{Int} and Ly6G^{Hi} neutrophils isolated from naïve mice following *ex vivo* culture. 1hr time-point n=8 mice; 4hr time-point n=8 mice; 20hr time-point n=8 mice. Data were analysed by 2way ANOVA with Tukey's multiple comparisons test. **g**, Heatmap showing row-scaled EdU^{+} as %Ly6G^{Int} and Ly6G^{Hi} neutrophils at 4, 12 and 24 hours post-EdU injection. BM: PBS 4hr, 12hr

and 24hr Ly6G^{Int} and Ly6G^{Hi} n=5 mice; CSF-3 4hr, 12hr and 24hr Ly6G^{Int} and Ly6G^{Hi} n=5 mice; LPS 4hr, 12hr and 24hr Ly6G^{Int} and Ly6G^{Hi} n=5 mice. Peripheral blood: PBS 4hr, 12hr and 24hr Ly6G^{Int} and Ly6G^{Hi} n=5 mice; CSF-3 4hr, 12hr and 24hr Ly6G^{Int} and Ly6G^{Hi} n=5 mice; LPS 4hr, 12hr and 24hr Ly6G^{Int} and Ly6G^{Hi} n=5 mice. **h**, Top 10 most enriched process networks from DEGs with increased expression in BM Ly6G^{Int} compared to BM Ly6G^{Hi} neutrophils in PBS-control mice. Data from transcriptomic analysis. **i**, Top 10 most enriched process networks from DEGs with increased expression in BM Ly6G^{Int} compared to BM Ly6G^{Hi} neutrophils from LPS-challenged mice. Data from transcriptomic analysis. **j**, Top 10 most enriched process networks from DEGs with increased expression in peripheral blood Ly6G^{Int} compared to peripheral blood Ly6G^{Hi} neutrophils from LPS-challenged mice. Data from transcriptomic analysis. **k**, Heatmap showing row scaled expression for genes associated with neutrophil maturation (identified by Xie *et al.,* 2020) for Ly6G^{Int} and Ly6G^{Hi} neutrophils in the peripheral blood (left) and BM (right). Data from transcriptomic analysis. **l**, Top 10 most enriched process networks from proteins with increased abundance in BM Ly6G^{Int} compared to BM Ly6G^{Hi} neutrophils from CSF-3-challenged mice. Data from proteomic analysis.

Bulk Ly6G^{Int} and Ly6G^{Hi} neutrophil RNA-Seq data in Fig. 2h-k. PBS BM: Ly6G^{Int} n=4 mice; Ly6G^{Hi} n=4 mice. LPS-BM: Ly6G^{Int} n=3 mice; Ly6G^{Hi} n=3 mice. PBS peripheral blood: Ly6G^{Hi} n=4 mice. LPS peripheral blood: Ly6G^{Int} n=4 mice; Ly6G^{Hi} n=4 mice. Bulk Ly6G^{Int} and Ly6G^{Hi} neutrophil proteomic data in Fig. 2l. CSF-3 BM Ly6G^{Int} n=3, and peripheral blood and BM Ly6G^{Hi} n=3 replicates. Each replicate composed of FACS isolated Ly6G^{Int} and Ly6G^{Hi} neutrophils pooled from n=4 mice. Dots in Fig. 2c-f represent individual mice. Error bars in Fig. 2c-f represent mean±SEM.

Differentially Expressed Genes (DEGs) increased in Ly6G^{Int} compared to Ly6G^{Hi} neutrophils were consistently enriched for cell cycle regulatory process networks in the BM and peripheral blood of PBS-control and LPS-challenged mice, confirming that these remain a more phenotypically immature population in the circulation (**Fig. 2h-j**). Using two recently identified gene signatures for stages of neutrophil development[8, 16] we positioned Ly6G^{Int} neutrophils between the promyelocyte and metamyelocyte stages in PBS-control and LPS-challenged mice (**Fig. 2k and Extended Data Fig. 2g**). Corroborating this, BM Ly6G^{Int} neutrophils from CSF-3-challenged mice were enriched in proteins involved in cell cycle regulation (**Fig. 2l**). Thus, Ly6G surface expression accurately identifies immature Ly6G^{Int} and mature Ly6G^{Hi} neutrophils in homeostasis and models of haematopoietic stress.

Other proposed markers of neutrophil maturity are altered in haematopoietic stress

Several other strategies have been proposed for measuring neutrophil maturity during homeostasis and/or particular disease models. We next sought to determine how generally applicable these markers are in non-tumour models by using CSF-3[22, 23] and LPS-challenge[24]. Using Ly6G surface expression as a reference point for neutrophil maturity, we investigated whether Ly6G^{Int} neutrophils could be identified as tdTomato$^{Dim/-}$ and Ly6G^{Hi} as tdTomato$^{Bright/+}$ using Catchup$^{IVM-red}$ mice in which *Ly6G-Cre* is used to drive tdTomato expression in neutrophils[25]. Ly6G^{+}tdTomato$^{Bright/+}$ cells composed a significantly higher percentage of Ly6G^{Hi} neutrophils

204 compared to their Ly6G^{Int} counterparts in the peripheral blood and BM of all models (**Fig. 3a and Extended**
205 **Data Fig. 3a**). However, CSF-3- and LPS-challenge significantly reduced the proportion of tdTomato$^{Bright/+}$
206 neutrophils (**Extended Data Fig. 3a, b**). Here, Ly6G^{Hi} neutrophils were as low as 60% tdTomato$^{Bright/+}$ in the
207 peripheral blood of LPS-challenged mice (**Fig. 3a**). Consequently, tdTomato intensity was not specific enough
208 to accurately determine neutrophil maturity during haematopoietic stress.

209 Cell surface CD101 expression has been proposed to distinguish between CD101^{-} immature and
210 CD101^{+} mature neutrophils[10]. Consistent with this, a significantly greater percentage of Ly6G^{Hi} neutrophils
211 were CD101^{+} compared to Ly6G^{Int} neutrophils in PBS-control mice (**Fig.3b and Extended Data Fig. 3c**).
212 However, neutrophil surface CD101 expression was drastically reduced in CSF-3- and LPS-challenge (**Fig. 3b,**
213 **c and Extended Data Fig. 3c**). EdU pulse-chase experiments identified BM neutrophil CD101 surface
214 expression occurs 36-48 hours after the last cell division, the same time as the appearance of EdU^{+}Ly6G^{+} in
215 the peripheral blood (**Fig. 3d, e**). Thus, CD101 surface expression occurs during the terminal stages of
216 neutrophil maturation and neutrophils can enter the blood prior to surface CD101 expression during
217 haematopoietic stress. Despite this, when cultured *ex vivo,* CD101^{-} neutrophils from LPS-challenged mice
218 upregulated CD101 surface expression between 8 and 24 hours, indicating that these neutrophils maintain
219 the potential to express CD101 outside of this inflammatory context (**Fig. 3f**). Combined Ly6G and c-Kit
220 (CD117) staining has also been used to identify neutrophil populations at distinct maturation stages in mice[14,
221 26] (**Extended Data Fig. 3d**). CD117 surface expression is restricted to BM Ly6G^{Int} neutrophils in PBS-controls
222 but is down-regulated in the BM and up-regulated by peripheral blood Ly6G^{Hi} neutrophils in CSF-3- and LPS-
223 challenged mice (**Extended Data Fig. 3d**). Using RNA-Seq analysis we confirmed transcriptional regulation
224 consistent with all of the findings above (**Fig. 3g**). Additionally, we identified stimulus dependent, variable
225 gene and protein expression for other potential markers of neutrophil maturity (e.g. *Cd48*[10], *Cd133*[27]) by
226 Ly6G^{Int} and Ly6G^{Hi} neutrophils (**Fig. 3g and Extended Data Fig. 3e**).

227 We next attempted to identify novel candidate cell surface markers of neutrophil maturity. Using
228 RNA sequencing (RNA-Seq) and gene ontology (GO) analysis, we found 19 DEGs between BM Ly6G^{Int} and
229 Ly6G^{Hi} neutrophils in PBS-control and LPS-challenged mice whose proteins localise to the external side of the
230 plasma membrane (GO:009897; **Fig. 3h**). Interrogating our proteomic dataset, we also identified 68 proteins

231 that localized within the plasma membrane with different abundance between Ly6G^{Int} and Ly6G^{Hi}

232 populations in CSF-3-challenged mice (**Fig. 3i**). However, the proteins identified included those that we and

233 others have shown to be unreliable markers of neutrophil maturity dependent on stimuli, including CD177[28],

234 CXCR2[10] and CD101. Therefore, as Ly6G expression closely matched objective measures of neutrophil

235 maturity and remained our most reliable indicator compared to all others tested, we subsequently refer to

236 Ly6G^{Int} neutrophils as 'immature' and Ly6G^{Hi} as 'mature' in the text.

237

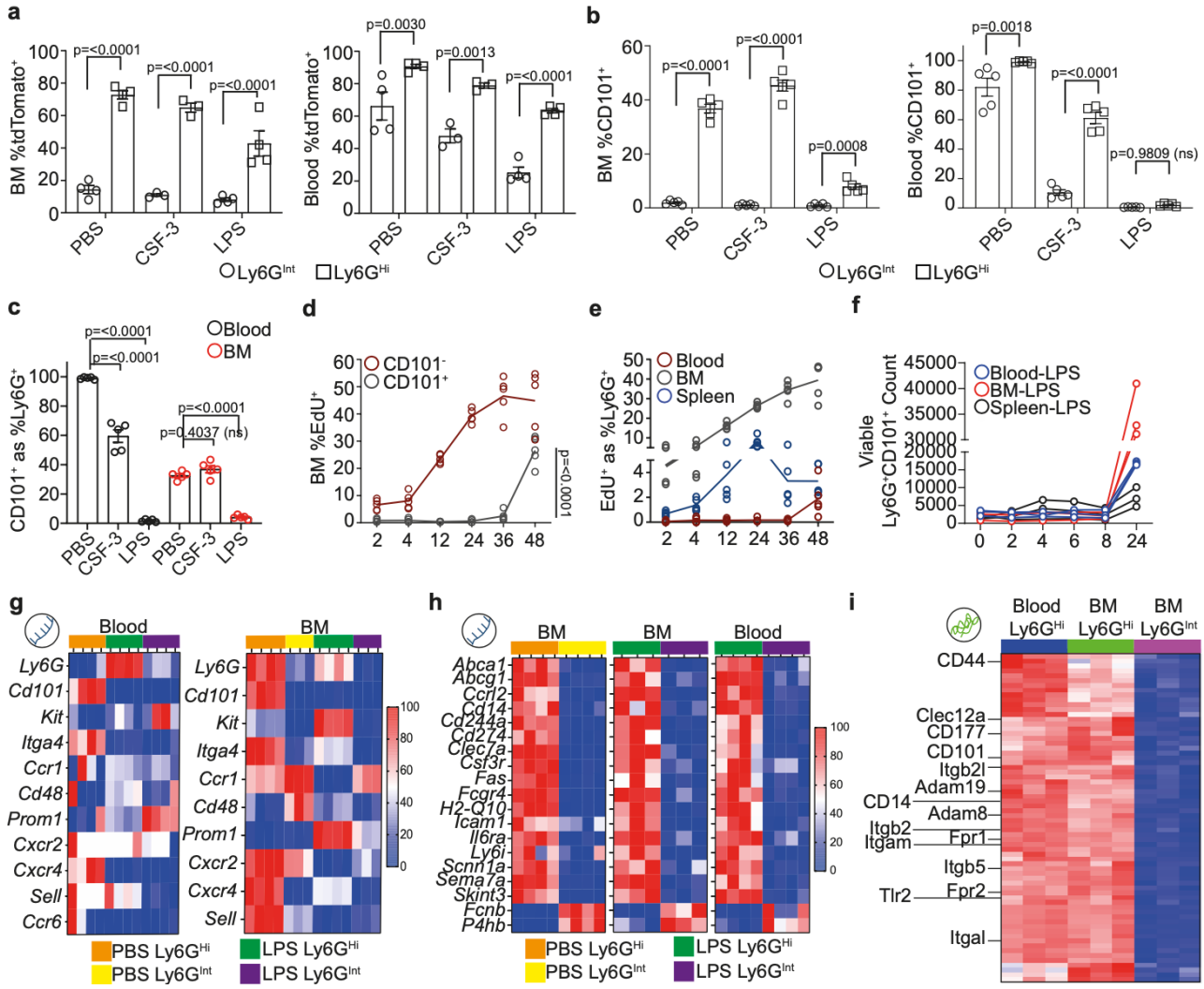

238

239 **Fig. 3. Alternative methods for identifying neutrophil maturity are less accurate in states of haematopoietic stress. a**,
240 Quantification of TdTomato^{+} as %Ly6G^{Int} and Ly6G^{Hi} neutrophils in the BM (left) and peripheral blood (right) of
241 Catchup$^{IVM\text{-}red}$ mice (developed by Hasenberg *et al.,* 2015). BM Ly6G^{Int} and Ly6G^{Hi} neutrophils: PBS n=4 mice; CSF-3 n=3
242 mice; LPS n=4 mice. Peripheral blood Ly6G^{Int} and Ly6G^{Hi} neutrophils: PBS n=4 mice; CSF-3 n=3 mice; LPS n=4 mice. Data
243 from BM and peripheral blood were analysed by 2way ANOVA with Sidak's multiple comparisons test. **b**, Quantification
244 of CD101^{+} as %Ly6G^{Int} and Ly6G^{Hi} neutrophils in the BM (left) and peripheral blood (right). BM Ly6G^{Int} and Ly6G^{Hi}
245 neutrophils n=5 mice in PBS, CSF-3 and LPS. Peripheral blood Ly6G^{Int} and Ly6G^{Hi} neutrophils n=5 mice in PBS, CSF-3 and
246 LPS. Data from BM and peripheral blood were analysed by 2way ANOVA with Sidak's multiple comparisons test. **c**,
247 Quantification of CD101^{+} as %Ly6G^{+} neutrophils. Peripheral blood and BM n=5 mice in PBS, CSF-3 and LPS. Data were
248 analysed by 2way ANOVA with Sidak's multiple comparisons test. **d**, Quantification of EdU^{+} as %CD101^{+} in the BM of
249 naïve mice at 2, 4, 12, 24, 36 and 48 hours post-EdU injection. CD101^{-} and CD101^{+} n=5 mice at all time-points. Data were

250 analysed by 2way ANOVA with Tukey's multiple comparisons test. **e**, Quantification of EdU$^+$ as %Ly6G$^+$ in the peripheral
251 blood, BM and spleen of naïve mice at 2, 4, 12, 24, 36 and 48 hours post-EdU injection. Peripheral blood, BM and spleen
252 Ly6G$^+$ neutrophils n=5 mice at all time-points. **f**, Quantification of the no. of viable Ly6G$^+$CD101$^+$ neutrophils isolated
253 from the peripheral blood, BM and spleen of LPS-challenged mice after 0, 2, 4, 6, 8 and 24 hours culture *ex vivo.*
254 Peripheral blood, BM and spleen Ly6G$^+$CD101$^+$ neutrophils n=3 mice at all time-points. **g**, Heatmap showing row scaled
255 expression for genes associated with proposed cell surface markers of neutrophil maturation. Data from transcriptomic
256 analysis. **h**, Heatmap showing row scaled expression for genes with proteins localized on the external side of the plasma
257 membrane (GO:0009897). Data from transcriptomic analysis. **i**, Heatmap showing row scaled protein abundance for
258 genes whose proteins are localized within the cell membrane and are increased in Ly6G^{Hi} compared to Ly6G^{Int}
259 neutrophils. Data from proteomic analysis.
260
261 Bulk Ly6G^{Int} and Ly6G^{Hi} neutrophil RNA-Seq data in Fig. 3g, h. PBS BM: Ly6G^{Int} n=4 mice; Ly6G^{Hi} n=4 mice. LPS-BM: Ly6G^{Int}
262 n=3 mice; Ly6G^{Hi} n=3 mice. PBS peripheral blood: Ly6G^{Hi} n=4 mice. LPS peripheral blood: Ly6G^{Int} n=4 mice; Ly6G^{Hi} n=4
263 mice. Bulk Ly6G^{Int} and Ly6G^{Hi} neutrophil proteomic data in Fig. 2l. CSF-3 BM Ly6G^{Int} n=3, and peripheral blood and BM
264 Ly6G^{Hi} n=3 replicates. Each replicate composed of FACS isolated Ly6G^{Int} and Ly6G^{Hi} neutrophils pooled from n=4 mice.
265 Dots in Fig. 3a-f represent individual mice. Error bars in Fig. 3a-c represent mean±SEM.
266
267

268 **Immature neutrophils have reduced immune regulatory and adhesion capacity**

269 As neutrophils develop effector mechanisms during maturation, for example neutrophil granules[29],
270 neutrophils at different maturation stages should have different functional capacity. Like transcriptomic
271 differences (**Extended Data Fig. 2e, f**), proteomic analysis identified a striking difference in protein content
272 of BM immature compared to BM and peripheral blood mature neutrophil populations (**Extended Data Fig.
273 4a**). Here, proteins increased in immature neutrophils were predominantly involved in DNA, RNA,
274 metabolism/catabolism and biosynthesis/building associated biological processes, consistent with our RNA-
275 Seq data (**Fig. 4a**). The proteins increased in mature neutrophils were preferentially involved in
276 adhesion/motility, regulation/signalling and cellular response associated biological processes and process
277 networks (**Fig. 4a, b**). LPS-challenge induced a clear shift in gene transcription by both immature and mature
278 neutrophils compared to PBS-controls, including down-regulation (e.g. *Cd101, Ptgs2, Cxcr1*) and up-
279 regulation (e.g. *Nos2, Ngp, Il10*) of genes (**Table 1, Fig. 4c and Extended Data Fig. 4b**). Despite this, the DEGs
280 increased in LPS-challenge peripheral blood mature neutrophils were also preferentially involved in immune
281 response regulation including phagocytosis and adhesion (**Extended Data Fig. 4c**).

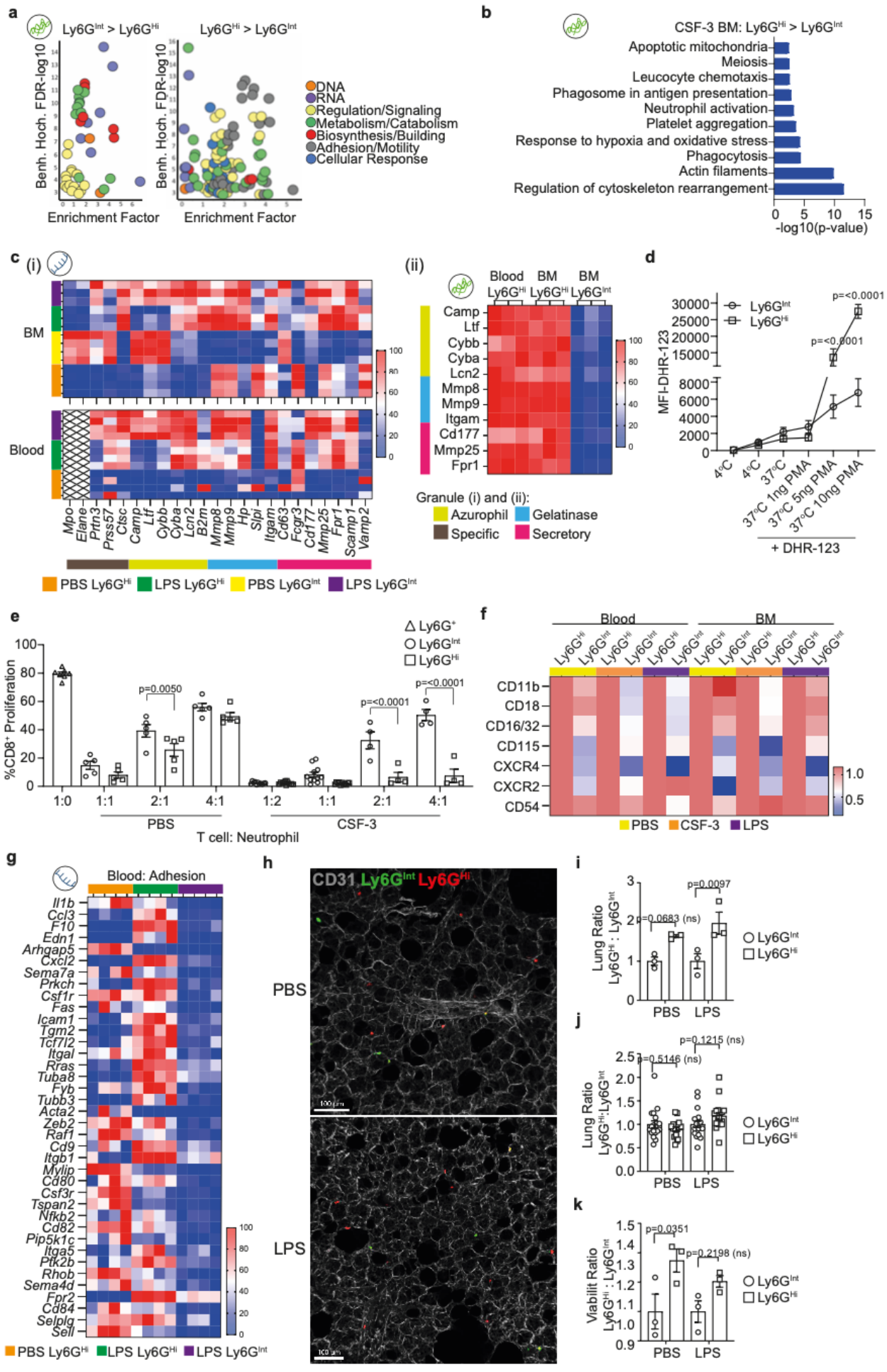
a
Ly6G^Int > Ly6G^Hi
Ly6G^Hi > Ly6G^Int
Benh. Hoch. FDR-log10
Enrichment Factor
DNA
RNA
Regulation/Signaling
Metabolism/Catabolism
Biosynthesis/Building
Adhesion/Motility
Cellular Response
b
CSF-3 BM: Ly6G^Hi > Ly6G^Int
Apoptotic mitochondria
Meiosis
Leucocyte chemotaxis
Phagosome in antigen presentation
Neutrophil activation
Platelet aggregation
Response to hypoxia and oxidative stress
Phagocytosis
Actin filaments
Regulation of cytoskeleton rearrangement
-log10(p-value)
c
(i)
BM
Blood
Mpo Elane Prtn3 Prss57 Ctsc Camp Ltf Cybb Cyba Lcn2 B2m Mmp8 Mmp9 Hp Slpi Itgam Cd63 Fcgr3 Cd177 Mmp25 Fpr1 Scamp1 Vamp2
PBS Ly6G^Hi
LPS Ly6G^Hi
PBS Ly6G^Int
LPS Ly6G^Int
(ii)
Blood Ly6G^Hi
BM Ly6G^Hi
BM Ly6G^Int
Camp
Ltf
Cybb
Cyba
Lcn2
Mmp8
Mmp9
Itgam
Cd177
Mmp25
Fpr1
Granule (i) and (ii):
Azurophil
Gelatinase
Specific
Secretory
d
Ly6G^Int
Ly6G^Hi
MFI-DHR-123
p=<0.0001
4°C
37°C
37°C 1ng PMA
37°C 5ng PMA
37°C 10ng PMA
+ DHR-123
e
Ly6G+
Ly6G^Int
Ly6G^Hi
%CD8+ Proliferation
p=0.0050
p=<0.0001
1:0
1:1
2:1
4:1
1:2
PBS
CSF-3
T cell: Neutrophil
f
Blood
BM
CD11b
CD18
CD16/32
CD115
CXCR4
CXCR2
CD54
PBS
CSF-3
LPS
g
Blood: Adhesion
Il1b
Ccl3
F10
Edn1
Arhgap5
Cxcl2
Sema7a
Prkch
Csf1r
Fas
Icam1
Tgm2
Tcf7l2
Itgal
Rras
Tuba8
Fyb
Tubb3
Acta2
Zeb2
Raf1
Cd9
Itgb1
Mylip
Cd80
Csf3r
Tspan2
Nfkb2
Cd82
Pip5k1c
Itga5
Ptk2b
Rhob
Sema4d
Fpr2
Cd84
Selplg
Sell
PBS Ly6G^Hi
LPS Ly6G^Hi
LPS Ly6G^Int
h
CD31 Ly6G^Int Ly6G^Hi
PBS
LPS
i
Lung Ratio Ly6G^Hi : Ly6G^Int
p=0.0683 (ns)
p=0.0097
PBS
LPS
j
Lung Ratio Ly6G^Hi:Ly6G^Int
p=0.5146 (ns)
p=0.1215 (ns)
k
Viabilit Ratio Ly6G^Hi : Ly6G^Int
p=0.0351
p=0.2198 (ns)

282

Fig. 4. Ly6G^{Int} neutrophils have reduced functional capacity compared to Ly6G^{Hi}. a, GO Biological Process clustering for proteins enriched in BM Ly6G^{Int} compared to Ly6G^{Hi} (left) and BM Ly6G^{Hi} compared to Ly6G^{Int} (right) from CSF-3-challenged mice. Data from proteomic analysis. **b**, Top 10 most enriched process networks from proteins with increased abundance in BM Ly6G^{Hi} compared to BM Ly6G^{Int} neutrophils from CSF-3-challenged mice. Data from proteomic analysis. **c**, Heatmap showing row-scaled (i) gene expression and (ii) protein abundance for neutrophil granule components. Data from (i) transcriptomic and (ii) proteomic analysis. **d**, Quantification of MFI for DHR-123 in *ex vivo* PMA stimulated Ly6G^{Int} and Ly6G^{Hi} neutrophils isolated from the BM of naïve mice. Data from flow cytometry analysis. Ly6G^{Int} and Ly6G^{Hi} neutrophils n=6 mice for each condition. Data were analysed by 2way ANOVA with Sidak's multiple comparisons test. **e**, Quantification of %CD8^{+} T cell proliferation when cultured *ex vivo* with Ly6G^{Int} or Ly6G^{Hi} neutrophils isolated from the BM of PBS-control or CSF-3-challenged mice, at different T cell: neutrophil ratios. Data from flow cytometry analysis. Ly6G^{+} neutrophils 1:0 ratio n=7 mice. Ly6G^{Int} and Ly6G^{Hi} neutrophils: PBS 1:1, 2:1 and 4:1 ratios n=5 mice; CSF-3 1:2 and 1:1 ratios n=11 mice; CSF-3 2:1 and 4:1 ratios n=4 mice. Data were analysed by 2way ANOVA with Sidak's multiple comparisons test. **f**, Heatmap showing row scaled CD11b^{+}, CD18^{+}, CD16/32^{+}, CD115^{+}, CXCR4^{+}, CXCR2^{+} and CD54 as %Ly6G^{Int} and Ly6G^{Hi} neutrophils isolated from the peripheral blood and BM of PBS-control, CSF-3- and LPS-challenged mice. Data from flow cytometry analysis. Data are shown as ratio between Ly6G^{Int} and Ly6G^{Hi} where Ly6G^{Hi} = 1. Peripheral blood and BM Ly6G^{Int} and Ly6G^{Hi} neutrophils: CD11b PBS n=8 mice, CSF-3 n=7 mice, LPS n=8 mice; CD18 PBS n= 5 mice, CSF-3 n=7 mice; LPS n=3 mice; CD16/32 PBS n=3 mice, CSF-3 n=3 mice, LPS n=3 mice; CD115 PBS n=3 mice, CSF-3 n=3 mice, LPS n=3 mice; CXCR4 PBS n=5 mice, CSF-3 n= 7 mice, LPS n=3 mice; CD54 PBS n=5 mice, CSF-3 n=4 mice, LPS n=5 mice; CXCR2 PBS n=3 mice, CSF-3 n=7 mice, LPS n=4 mice. **g**, Heatmap showing row-scaled expression for genes associated with leukocyte adhesion in peripheral blood Ly6G^{Int} and Ly6G^{Hi} neutrophils. Data from transcriptomic analysis. **h**, Confocal images of adoptively transferred Ly6G^{Int} and Ly6G^{Hi} neutrophils in the lungs of PBS-control and LPS-challenged recipient mice. Data representative of PBS n=3 mice and LPS n=3 mice. **i**, Quantification of adoptively transferred Ly6G^{Int} and Ly6G^{Hi} neutrophils recovered from the right lung lobe of recipient mice, expressed as a fold change per replicate mouse for Ly6G^{Int} over Ly6G^{Hi}. Data from flow cytometry analysis. PBS n=3 mice; LPS n=3 mice. Data were analysed by 2way ANOVA with Sidak's multiple comparisons test. **j**, Quantification of the number of adoptively transferred Ly6G^{Int} and Ly6G^{Hi} neutrophils identified in precision cut lung slices (PCLS) of recipient mice by confocal microscopy, expressed as a ratio between Ly6G^{Int}: Ly6G^{Hi}. PBS n=3 mice; LPS n=3 mice. From each mouse 2x images from 3x PCLS were analysed. Data were analysed by 2way ANOVA with Sidak's multiple comparisons test. **k**, Viability of Ly6G^{Int} and Ly6G^{Hi} neutrophils recovered from the right lung lobe of recipient mice, expressed as a fold change per replicate mouse for Ly6G^{Int} over Ly6G^{Hi}. Data from flow cytometry analysis. PBS n=3 mice; LPS n=3 mice. Data were analysed by 2way ANOVA with Sidak's multiple comparisons test.

Bulk Ly6G^{Int} and Ly6G^{Hi} neutrophil RNA-Seq data in Fig. 4c(i), g. PBS BM: Ly6G^{Int} n=4 mice; Ly6G^{Hi} n=4 mice. LPS-BM: Ly6G^{Int} n=3 mice; Ly6G^{Hi} n=3 mice. PBS peripheral blood: Ly6G^{Hi} n=4 mice. LPS peripheral blood: Ly6G^{Int} n=4 mice; Ly6G^{Hi} n=4 mice. Bulk Ly6G^{Int} and Ly6G^{Hi} neutrophil proteomic data in Fig. 2l. CSF-3 BM Ly6G^{Int} n=3, and peripheral blood and BM Ly6G^{Hi} n=3 replicates. Each replicate composed of FACS isolated Ly6G^{Int} and Ly6G^{Hi} neutrophils pooled from n=4 mice. Dots in Fig. 4d represent averages. Dots in Fig. 4e, i, k represent individual mice. Dots in Fig. 4j represent individual images from PCLS. Error bars in Fig. 4d, e, i-k represent mean±SEM.

Whereas BM immature neutrophils from PBS-control mice had increased transcription of azurophil and gelatinase granule-associated genes (**Fig. 4c(i)**), immature neutrophils from the BM and peripheral blood of LPS-challenged mice had increased transcription of genes associated with all granule types consistent with a more rapid maturation phenotype following LPS-challenge (**Fig. 4c(i)**). Consistently, proteomics showed that immature neutrophils had reduced levels of specific, gelatinase and secretory granule proteins (**Fig. 4c(ii)**).

We next sought to investigate the functional capacity of immature and mature neutrophils. Proteomic analysis revealed that NADPH-components were reduced in immature compared to mature neutrophils (**Extended Data Fig. 4d**). *Ex vivo* quantification of intracellular ROS with DHR-123 identified a

331 slight increase in intracellular ROS production at 4°C, 37°C and 37°C with 1ng PMA stimulation by immature
332 neutrophils (**Fig. 4d**). In contrast, the intracellular oxidative burst was far greater in mature neutrophils when
333 stimulated with more PMA (**Fig. 4d and Extended Data Fig. 4e**). Neutrophils have been shown to suppress T
334 cells in several disease contexts and maturity has been implicated in their suppressive capacity[4]. However,
335 both immature and mature neutrophils from control mice suppressed $CD8^+$ and $CD4^+$ T cell proliferation and
336 reduced their viability in a ratio-dependent manner (**Fig. 4e and Extended Data Fig. 4f-h**). This effect was
337 stronger when using mature compared to immature neutrophils and was further augmented when T cells
338 were cultured with mature neutrophils isolated from the BM of CSF-3-treated mice (**Fig. 4e and Extended**
339 **Data Fig. 4g, h).** This suggests that the environment the cells are taken from plays a role in this behaviour
340 rather than maturity alone, and that immature and mature neutrophils can have a different functional
341 response to the same environment (**Fig. 4e and Extended Data Fig. 4g, h**).

342 We found that cell membrane localized adhesion and cell-cell interaction associated (e.g. ITGAM,
343 CD11b; ITGAL, CD11a; ITGB2, CD18; ITGB2L; ITGB5; CD177; CD44; CLEC12a; ADAM19; ADAM8) and pathogen
344 detection (e.g. CD14, TLR2, FPR1, FPR2) proteins were highly represented in mature neutrophils (**Fig. 3i and**
345 **Fig. 4f**). In the peripheral blood of LPS-challenged mice, immature neutrophils had reduced gene expression
346 of adhesion associated genes compared to mature ones (**Fig. 4g**). Flow cytometry confirmed lower surface
347 expression of adhesion molecules (CD11b, CD18, CD54) and chemokine receptors (CXCR2, CXCR4) by
348 immature neutrophils (**Fig. 4f**). These data are consistent with immature neutrophils having a
349 reduced/altered effector capacity compared to their mature counterparts and emphasise their plasticity to
350 develop the proteins needed during maturation, and also in response to stimuli, rather than being equipped
351 with a fixed set at early stages. We next sought to test for consequent reduced adhesion of immature
352 neutrophils *in vivo*. During sepsis, neutrophil retention in the lung can promote acute respiratory distress
353 syndrome (ARDS), worsening pathology[30]. In mice, systemic LPS-challenge is commonly used to model sepsis-
354 induced ARDS[31, 32]. To obtain large enough numbers, BM-derived immature and mature neutrophil
355 populations were sorted from CSF-3-challenged mice and intravenously (i.v.) adoptively transferred into PBS-
356 control or LPS-challenged mice. Fewer adoptively transferred immature neutrophils were detected in the
357 lungs of PBS-control and LPS-challenged mice compared to mature neutrophils when analysed by flow

358 cytometry and microscopy of precision cut lung slices (**Fig. 4h-j**). Furthermore, adoptively transferred
359 immature neutrophils had reduced viability compared to mature neutrophils (**Fig. 4k**). Together, these data
360 indicate that immature neutrophils are less capable at adhesion, migration, trafficking, pathogen removal,
361 ROS production, and T cell suppression based on transcriptomic, proteomic, and flow cytometric, in addition
362 to *in vivo* and *ex vivo* functional assays.
363
364 **Homeostatic neutrophil development in the spleen is distinct from the BM**
365 Neutrophil tissue localization can influence their gene expression[3, 9]. Consistent with this, when we compared
366 neutrophils isolated from separate tissues, immature and mature neutrophils had unique transcriptional
367 profiles compared to the same maturation stage in other sites (**Table 2-4 and Fig. 5a**). Interestingly, while
368 LPS-challenge induced a clear shift in the expression profile of both immature and mature neutrophils
369 isolated from the same tissue compared to PBS-controls (PC2 variance 27.4%), variance between neutrophils
370 isolated from separate tissues was greater (PC1 variance 49.5%; **Fig. 5a**). Furthermore, tissue variance was
371 only slightly reduced in LPS-challenged mice compared to PBS-controls, indicating tissue specific signatures
372 are largely maintained in acute inflammation (**Fig. 5a**).
373 Immature neutrophils were enriched in the spleen compared to other peripheral tissues and
374 peripheral blood in control animals (**Fig. 5b, Fig. 1l-p (WT mice) and Extended Data Fig. 5a**) consistent with
375 other reports of their presence in a steady state[5]. In the spleen of naïve mice, we found clusters of
376 morphologically banded neutrophils localized in the red-pulp and using flow cytometry we identified
377 unipotent neutrophil progenitors, termed NePs[33] (**Fig. 5c and Extended Data Fig. 5b**). We next investigated
378 whether tissue specific factors altered splenic neutrophil maturation compared to the BM. Similarly to the
379 BM, splenic immature neutrophils had a different expression profile to mature neutrophils, enriched DEGs
380 preferentially involved in cell cycle regulation compared to mature neutrophils, and were positioned
381 between myelocyte and metamyelocytes using the 24 maturation stage-associated genes as above[16] (**Fig. 5d,**
382 **e and Extended Data Fig. 5c**). Additionally, as we had seen before in the BM, LPS-challenge increased
383 expression of genes associated with later maturation stages, and the immature splenic neutrophils rapidly

incorporated EdU within 2-4 hours of its injection, and contained Ki67^{+} cells in PBS-control, CSF-3- and LPS-challenged mice (**Fig. 5e-g and Extended Data Fig. 5d, e**).

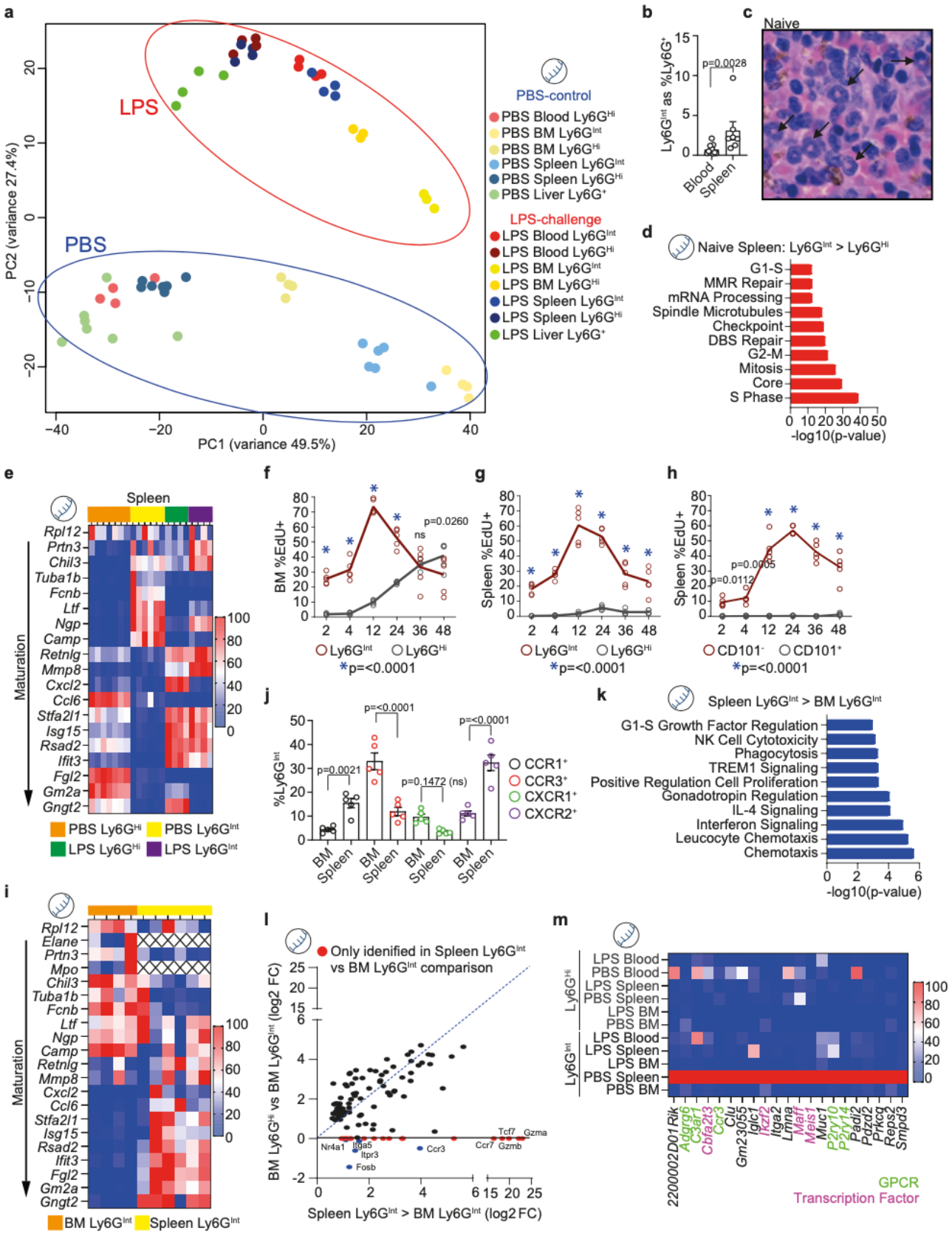

Fig. 5. Splenic neutrophil maturation is distinct from the BM. a, PCA plot for Ly6G^{+}, Ly6G^{Int} and Ly6G^{Hi} transcriptomic analysis from the peripheral blood, BM, spleen and liver of PBS-control and LPS-challenged mice. **b,** Quantification of

389 Ly6G^{Int} as %Ly6G^{+} in the peripheral blood and spleen of naïve mice. Peripheral blood n=11 mice; spleen n=7 mice. Data
390 were analysed by Mann-Whitney test. **c**, H&E identification of banded neutrophils in the splenic red pulp of naïve mice.
391 Data representative of n=5 mice. Black arrows indicate banded neutrophils. **d**, Top 10 most enriched Process Networks
392 from DEGs with increased expression in spleen Ly6G^{Int} compared to spleen Ly6G^{Hi} neutrophils from naive mice. Data
393 from transcriptomic analysis. **e**, Heatmap showing row scaled expression for genes associated with neutrophil
394 maturation (identified by Xie *et al.,* 2020) for Ly6G^{Int} and Ly6G^{Hi} neutrophils in spleen. Data from transcriptomic analysis.
395 **f**, Quantification of EdU^{+} as %Ly6G^{Int} and Ly6G^{Hi} neutrophils in the BM of naïve mice. Ly6G^{Int} and Ly6G^{Hi} neutrophils n=5
396 mice at each time-point. Data were analysed by 2way ANOVA with Sidak's multiple comparisons test. Blue star (*)
397 indicates comparisons with p-value<0.0001. For 'ns' at 36hr time-point, p-value=0.9989. **g**, Quantification of EdU^{+} as
398 %Ly6G^{Int} and Ly6G^{Hi} neutrophils in the spleen of naïve mice. Ly6G^{Int} and Ly6G^{Hi} neutrophils n=5 mice at each time-point.
399 Data were analysed by 2way ANOVA with Sidak's multiple comparisons test. Blue star (*) indicates comparisons with p-
400 value<0.0001. **h**, Quantification of EdU^{+} as %CD101^{-} and CD101^{+} neutrophils in the spleen of naïve mice. CD101^{-} and
401 CD101^{+} neutrophils n=5 mice at each time-point. Data were analysed by 2way ANOVA with Sidak's multiple comparisons
402 test. Blue star (*) indicates comparisons with p-value<0.0001. **i**, Heatmap showing row scaled expression for genes
403 associated with neutrophil maturation (identified by Xie *et al.,* 2020) for Ly6G^{Int} neutrophils in BM and spleen from naïve
404 mice. Data from transcriptomic analysis. **j**, Quantification of CCR1^{+}, CCR3^{+}, CXCR1^{+} and CXCR2^{+} as %Ly6G^{Int} neutrophils
405 in the BM and spleen of naïve mice. Data from flow cytometry analysis. BM Ly6G^{Int} n=5 mice; spleen Ly6G^{Int} n=5 mice.
406 Data were analysed by 2way ANOVA with Sidak's multiple comparisons test. **k**, Top 10 most enriched Process Networks
407 from DEGs with increased expression in spleen Ly6G^{Int} compared to BM Ly6G^{Int} neutrophils from naive mice. Data from
408 transcriptomic analysis. **l**, Correlation for genes identified in process networks from **Fig. 5k** between spleen Ly6G^{Int} and
409 BM Ly6G^{Hi}, shown as log2 fold change (FC) compared to BM Ly6G^{Int}. Data from transcriptomic analysis. **m**, Heatmap
410 showing column scaled expression for genes with high expression unique to spleen Ly6G^{Int} neutrophils. Data from
411 transcriptomic analysis.
412
413 Bulk Ly6G^{+}, Ly6G^{Int} and Ly6G^{Hi} neutrophil RNA-Seq data in Fig. 5a, d, e, i, k-m. PBS: peripheral blood Ly6G^{Hi} n=4 mice;
414 BM Ly6G^{Int} n=4 mice; BM Ly6G^{Hi} n=4 mice; spleen Ly6G^{Int} n=6 mice; spleen Ly6G^{Hi} n=7 mice; liver Ly6G^{+} n=7 mice. LPS:
415 peripheral blood Ly6G^{Int} n=4 mice; peripheral blood Ly6G^{Hi} n=4 mice; BM Ly6G^{Int} n=3 mice; BM Ly6G^{Hi} n=3 mice; spleen
416 Ly6G^{Int} n=4 mice; spleen Ly6G^{Hi} n=4 mice; liver Ly6G^{+} n=4 mice. Dots in Fig. 5a, b, f-h, j represent individual mice. Error
417 bars in Fig. 5b, f-h, j represent mean±SEM.
418 _____
419

420 In the BM, EdU^{+} immature neutrophils increased from 2-12 hours and reduced from 12-48 hours post-EdU
421 pulse, coincident with an increase in EdU^{+} mature neutrophils consistent with Ly6G surface upregulation with
422 maturation (**Fig. 5f**). However, although splenic EdU^{+} immature neutrophils increased from 2-12 hours and
423 reduced between 12-48 hours post-injection, there was no coincident increase in EdU^{+} mature neutrophils
424 (**Fig. 5g**). As in the BM CD101 surface expression occurred during the terminal stages of neutrophil maturation
425 (**Fig. 3d**) we analysed CD101 expression in the spleen to explore whether splenic post-mitotic transit time
426 was shorter when compared to the BM. We observed no significant increase in EdU^{+}CD101^{+} neutrophils in
427 the spleen up to 48 hours post-injection and only observed EdU^{+}CD101^{+} neutrophils in the peripheral blood
428 between 36-48 hours corresponding with their emergence from the BM (**Fig. 5h and Extended Data Fig. 5f**).
429 As the spleen also clears neutrophils from the circulation[34], we analysed pro-apoptotic genes (GO:0043065)
430 in splenic immature neutrophils compared to other populations. As expected, mature neutrophils generally
431 expressed these genes at higher levels than immature, but specifically, immature neutrophils in the spleen

432 were not enriched for these suggesting that they do not apoptose there (**Extended Data Fig. 5g**). The BM
433 contains a neutrophil reserve composed of mature, terminally differentiated neutrophils that can be rapidly
434 mobilized in response to stress. The spleen has been proposed to contain marginated neutrophils, however,
435 we found no evidence in the literature for a distinct splenic-neutrophil reserve analogous to that in the BM[35].
436 Therefore, we interpret these data as confirming the presence of an abundant splenic immature neutrophil
437 population that is released earlier from its developmental niche, compared to those in the BM, which enter
438 the BM reserve.
439
440 **Splenic-derived neutrophils have quicker maturation and altered transcriptional phenotype**
441 Recently developed mature neutrophils form the BM-reserve and undergo important changes associated
442 with their functional capacity, including their development of secretory vesicles[7]. To investigate whether
443 maturation was faster in splenic- compared to BM-derived neutrophils to account for the absence of a
444 splenic-reserve, we compared BM and spleen immature neutrophil gene expression profiles (**Table 2**). Splenic
445 immature neutrophils had increased expression of later stage maturation genes compared to BM immature
446 neutrophils in PBS-control mice (**Fig. 5i and Extended Data Fig. 5h**). Furthermore, spleen immature
447 neutrophils had significantly different mRNA levels for several chemokine receptors (**Extended Data Fig. 5i**).
448 Flow cytometry confirmed a significant increase in CCR1 and CXCR2, and a significant decrease in CCR3
449 surface expression, by splenic immature compared to BM immature neutrophils in naïve mice (**Fig. 5j**). In
450 mature neutrophils, the percentage $CCR1^+$ and $CXCR2^+$ cells increased, and $CCR3^+$ decreased, from BM to
451 spleen to peripheral blood respectively (**Extended Data Fig. 5j**). When we directly compared BM and spleen
452 immature neutrophils, we found those from BM were enriched in genes associated with cell cycle regulation
453 and those from the spleen were enriched in inflammatory/immune response networks (**Fig. 5k and Extended**
454 **Data Fig. 5k**). This closely matched genes associated with these process networks that were enriched in BM
455 mature neutrophils compared to BM immature neutrophils, including interferon signalling (**Fig. 5l and**
456 **Extended Data Fig. 5l**). However, expression of certain genes (*Nr4a1, Itga5, Itpr3, Ccr3, Fosb*) increased in
457 spleen immature neutrophils had reduced expression in the BM mature-immature comparison and some
458 were unique to spleen immature neutrophils (e.g. *Gzma, Gzmb, Tcf7, Ccr7*; **Fig. 5l**). We also identified several

459 genes with high expression unique to PBS-control spleen immature neutrophils including GPCRs (e.g. *C3ar1,*
460 *Pr2y10*) and transcription factors (e.g. *Ikzf2, Maff*; **Fig. 5m**). Together, these data are consistent with a quicker
461 maturation phenotype, shorter post-mitotic transit and earlier release from the splenic developmental niche
462 compared to neutrophils that originate in the BM, in addition to a unique splenic developmental-niche driven
463 expression signature.
464
465 **Splenic-granulopoiesis remains distinct from the BM in tumour bearing mice**
466 As previously shown, immature neutrophils were identified in the spleen of DEN/ALIOS, KPN, KC, KP^{fl}C and
467 KPC mice (**Fig. 1**). This was confirmed histologically by clusters of banded neutrophils localized in the splenic
468 red-pulp (**Fig. 6a**). As splenic immature neutrophils were abundant in both highly metastatic models
469 analysed, we next investigated if the presence of a PDAC and metastatic potential influences BM and spleen
470 immature neutrophil phenotype. RNA-Seq of BM and splenic neutrophils isolated from WT, KP^{fl}C and KPC
471 mice confirmed an enrichment in genes associated with cell cycle regulation in BM and spleen immature
472 compared to mature neutrophils (**Fig. 6b and Extended Data Fig. 6a**). The presence of a PDAC led to a
473 dramatic shift in expression in BM and spleen immature neutrophils associated with an increased activated
474 degranulatory phenotype (**Table 5, 6; Fig. 6c; Extended Data Fig. 6b**). However, direct comparison of BM and
475 spleen immature neutrophils between KP^{fl}C and KPC genotypes identified 1 (*Eps8l1*) and 0 DEGs, respectively
476 (**Table 5, 6**). Despite this, in the BM we identified 88 DEGs unique to KP^{fl}C, 267 DEGs unique to KPC and 187
477 DEGs shared by KP^{fl}C and KPC BM immature neutrophils compared to those in WT mice (**Table 7**). In the
478 spleen we identified 204 DEGs unique to KP^{fl}C, 916 DEGs unique to KPC and 504 DEGs shared by KP^{fl}C and
479 KPC spleen immature neutrophils compared to WT (**Table 7**). We interpret the absence of DEGs between
480 KP^{fl}C and KPC, but increased number of DEGs between KPC compared to WT, as indicating a progressive gene
481 expression profile from KP^{fl}C to KPC in both the BM and the spleen (**Extended Data Fig. 6c**). Immature
482 neutrophils from the BM and spleen of KPC mice have increased neutrophil activation associated gene
483 expression over KP^{fl}C compared to WT mice (**Fig. 6d**). Thus, while metastatic potential enhances splenic
484 granulopoiesis it does not significantly alter the splenic or BM developmental phenotype, rather the presence
485 of a PDAC promotes an enhanced neutrophil activation developmental phenotype.

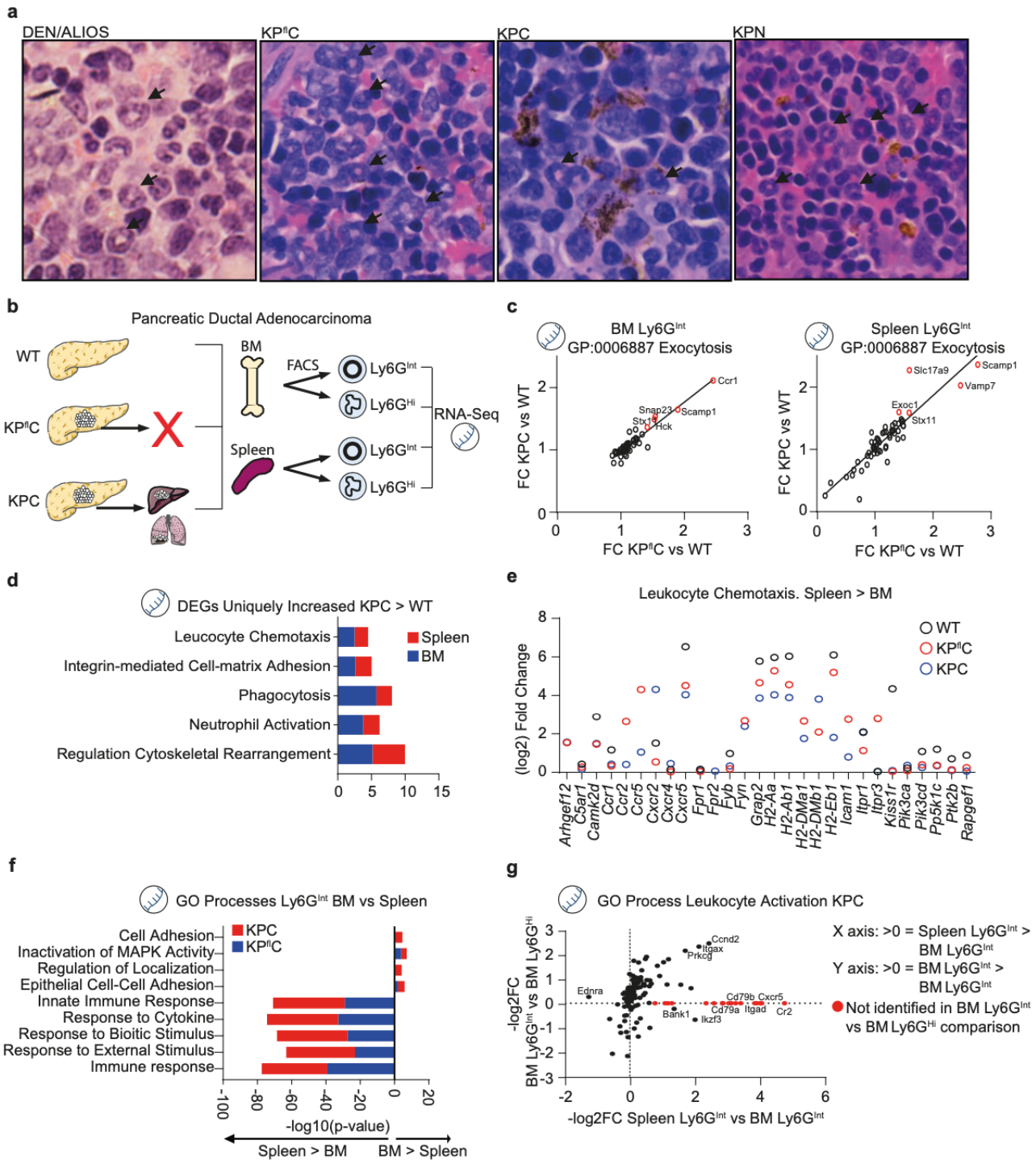

Fig. 6. Splenic Ly6G^{Int} neutrophils maintain a distinct maturation phenotype in tumour bearing mice. a, H&E identification of banded neutrophils in the splenic red pulp of DEN/ALIOS, KP^{fl}C, KPC and KPN mice. Data representative of DEN/ALIOS n=5 mice; KP^{fl}C n=5 mice, KPC n=5 mice and KPN n=5 mice. **b**, Schematic for RNA-Seq of BM and spleen Ly6G^{Int} and Ly6G^{Hi} neutrophil populations from WT controls, KP^{fl}C non-metastatic and KPC pre-metastatic mouse models of PDAC. **c**, Correlation for genes associated with exocytosis (GO:0006887) between KP^{fl}C and KPC Ly6G^{Int} neutrophils in the BM (left) and spleen (right), shown as fold change compared to WT Ly6G^{Int} neutrophils. Data from transcriptomic analysis. **d**, Process Networks associated with neutrophil activation enriched from DEGs uniquely increased in KPC compared to WT BM and spleen. Data from transcriptomic analysis. **e**, DEGs associated with leukocyte chemotaxis with increased expression in spleen Ly6G^{Int} compared to BM Ly6G^{Int} in WT, KP^{fl}C and KPC mice, shown as Log2 fold change. Data from transcriptomic analysis. **f**, GO Processes enriched from DEGs identified between KP^{fl}C and KPC BM Ly6G^{Int} and spleen Ly6G^{Int} neutrophils. Data from transcriptomic analysis. **g**, Correlation for genes associated with leukocyte activation (GO:0045321) between spleen Ly6G^{Int} and BM Ly6G^{Hi}, shown as Log2 fold change compared to BM Ly6G^{Int}. Data from transcriptomic analysis.

Bulk Ly6G^{Int} and Ly6G^{Hi} neutrophil RNA-Seq data in Fig. 5c-g. BM: WT Ly6G^{Int} n=10 mice; KP^{fl}C Ly6G^{Int} n=5 mice; KPC Ly6G^{Int} n=5 mice; KPC Ly6G^{Hi} n=5 mice. Spleen: WT Ly6G^{Int} n=8 mice; KP^{fl}C Ly6G^{Int} n=4 mice; KPC Ly6G^{Int} n=5 mice.

We next examined if BM and spleen immature neutrophils maintain their steady state differences in PDAC bearing mice. Splenic immature neutrophils from WT, KP^{fl}C and KPC mice had an increased expression of chemotaxis associated genes and advanced maturation signature compared to BM immature neutrophils (**Fig. 6d, e and Extended Data Fig. 6d**). However, the presence of a PDAC reduced the total number of DEGs between BM and spleen immature neutrophils in part due to reduced expression of developmental associated genes in BM immature neutrophils (**Table 8 and Extended Data Fig. 6e, f**). Despite this, spleen immature neutrophils maintained an increase in immune responsiveness gene expression compared to those in the BM of PDAC-bearing mice (**Fig. 6f**). Similar to steady state, BM mature, and spleen immature neutrophils, had a more similar expression profile to each other when compared to BM immature neutrophils, such as for those involved in leukocyte activation (e.g. *Ccand2, Itgax, Prkcg*), while many genes were unique to spleen immature neutrophils (e.g. *Cxcr5, Itgad*; **Fig. 6g**). Thus, as in homeostasis, spleen immature neutrophils maintain a more mature expression profile compared to BM immature neutrophils with some distinct characteristics compared to both BM immature and mature populations. We next investigated if BM and spleen immature neutrophils undergo different changes in PDAC bearing mice when compared to WT. DEGs shared by KP^{fl}C and KPC compared to WT from each tissue included 65 shared, 122 and 438 DEGs unique to BM and spleen immature neutrophils, respectively (**Extended Data Fig. 6g**). Here, the presence of a PDAC promoted an enhanced activated expression signature of splenic immature compared to BM immature neutrophils including increased expression of genes associated with antigen presentation (*Cd74, Cd79*) and immunosuppression (*Cd274, Btla*; **Extended Data Fig. 6h**). Therefore, differences likely to be functionally important between BM and spleen immature neutrophils are maintained in cancer models, but importantly, the increased abundance of these cells in cancer may enhance their functional consequences.

529 **Discussion**

530 Neutrophils are promising targets for therapeutic intervention[36, 37], however, due to their importance in
531 antimicrobial defence, it is vital to target these therapies only at the neutrophils that are detrimental in
532 disease. Immature neutrophils have been implicated in disease progression in a range of pathologies
533 including sepsis and cancer[11, 15] where they have been associated with immune suppression[4], tumour
534 burden[10] and metastasis[38]. Thus, characterising immature neutrophils and their contribution to neutrophil
535 heterogeneity is vital to efficiently targeting neutrophils in disease. We found that neutrophils expressing
536 intermediate levels of Ly6G, variably abundant in poorly metastatic mouse cancer models, were enriched in
537 two different spontaneously metastatic models. In the present study, we show that Ly6G expression level
538 accurately identifies neutrophil immaturity by morphological, flow cytometric, transcriptomic, and
539 proteomic analysis. This identification maintained its accuracy in homeostasis, experimental acute
540 haematopoietic stress and chronic haematopoietic stress caused by cancer, across multiple tissues, and
541 between different mouse strains, in contrast to other proposed maturity markers. Immature neutrophils
542 have been proposed to have altered function compared to their mature counterparts as a direct result of
543 their developmental status, including metabolic[14, 38], immuno-suppressive[39] and migratory[10] capacity.
544 Immature (Ly6G^{Int}) neutrophils had reduced granule composition, ROS production following activation,
545 suppressive capacity, cytoskeletal remodelling, and adhesion- and recruitment-associated proteins
546 compared to mature (Ly6G^{Hi}) neutrophils. Accordingly, fewer immature neutrophils were retained in the
547 lungs of PBS- and LPS-challenged mice confirming reduced adhesion with potential implications in disease
548 progression.

549 Extramedullary haematopoiesis (EMH) occurs physiologically in mice and is observed pathologically
550 in both mice and humans. Consistent with the literature[5], spleen immature neutrophils had increased
551 proliferative and reduced immune response capacity compared to spleen mature neutrophils. However, our
552 data positioned spleen immature neutrophils at a similar maturation stage to mature neutrophils in the BM
553 reserve. Furthermore, increased expression of chemokine receptors, release prior to CD101 surface
554 expression, and reduced cell cycle-associated gene expression are consistent with faster neutrophil
555 maturation in the spleen than in the BM. Tissue localization can influence the neutrophil transcriptome[3] and

556 neutrophils can display tissue specific properties in mice and humans, including in the spleen[40]. We found
557 that when compared to those from the BM, spleen immature neutrophils had distinct gene signatures that
558 were associated with altered immune and transcriptional regulation. Thus, the site of haematopoietic origin
559 influences neutrophil transit, maturation and functional characteristics even in a steady state. We propose
560 that these data signify that spleen immature neutrophils are pre-potentiated 'rapid responders' following
561 insult, more akin to reserve mature than immature neutrophils in the BM. It is anticipated that circulation of
562 BM-derived progenitors in a steady state[41] and disease promotes their seeding in the spleen, enhancing
563 extramedullary myelopoiesis[42]. Differences observed between BM- and spleen-derived neutrophils likely
564 arose from niche-induced alterations to development, similar to tissue-specific neutrophil phenotypes[3, 43, 44].
565 Spleen-derived neutrophils contribute to the systemic pool in sterile chronic inflammation[45] and
566 cancer where they can acquire an immunosuppressive state[44, 46]. The spleen is a major site of extramedullary
567 myelopoiesis in certain cancers and offers a potential therapeutic target[47]. Splenic-derived neutrophils can
568 promote tumour progression[44] and splenectomy can reduce metastatic burden[48]. We found that neutrophils
569 were markedly increased in the peripheral blood and spleen, occupying large clusters in the splenic red-pulp,
570 of highly metastatic CRC and PDAC mouse models. Here, we found that splenic immature neutrophils
571 maintained their distinct expression phenotype associated with increased chemotaxis and immune
572 responsiveness compared to BM immature neutrophils. Therefore, as metastasis is closely associated with
573 patient mortality in cancer[49] we postulate an important role for these abundant immature and splenic-
574 derived neutrophils in cancer progression. Our data also indicate that developmental origin is critical in
575 controlling neutrophil maturation and determining phenotype and function. However, EMH can occur at
576 multiple sites in cancer[50] and in other pathologies[51] raising the potential for a plethora of phenotypically and
577 functionally distinct neutrophil populations, on which deeper information is critical for the more specific
578 targeting of neutrophils in disease.
579
580
581
582

583 **Methods**

584 **Mouse strains**

585 All mice were housed in specific pathogen free conditions with unrestricted access to food and water and
586 maintained on a constant 12hr light/dark cycle under controlled climate (19-22°C, 45-65% humidity) at the
587 CRUK Beatson Institute, Glasgow or Imperial College London. All experiments involving mice were performed
588 in accordance with the UK Animal (Scientific Procedures) Act 1986, approved by the local animal welfare
589 (AWERB) committee and conducted under UK Home Office licences: 70/7463; 70/8377; PP3908577;
590 PE47BC0BF; PP6345023, and were compliant with the ARRIVE guidelines (https://www.nc3rs.org.uk/arrive-
591 guidelines). For all experiments using WT C57BL/6 mice, 8-12 week old mice were used. C57BL/6 mice were
592 purchased from Charles River Laboratories. Catchup$^{IVM\text{-}red}$ mice, as first described[25], were identified as
593 *Ly6G*$^{Cre\text{-}Rtom/+}$ *ROSA26*$^{Rtom/+}$ and were bred in-house and used for experiments when they were 8-15 weeks
594 old. For the metastatic model of CRC, KPN (*Villin*Cre^{ER}; *Kras*$^{G12D/+}$; *Trp53*$^{fl/fl}$; *Rosa26*$^{N1icd/+}$) mice[17], were used.
595 Mice of both sexes were induced with a single dose of 2mg tamoxifen (Sigma-Aldrich) by i.p. injection at 6-
596 12 weeks old. Mice were sampled at humane clinical endpoint by weight loss and/or hunching and/or
597 cachexia. For the DEN/ALIOS model of HCC, male WT C57BL/6 mice received a single dose of
598 diethylnitrosamine (DEN; 80mg/kg) by intraperitoneal (i.p.) injection at 14 days old and were subsequently
599 fed an American Lifestyle Induced Obesity Syndrome (ALIOS) diet (Envigo, TD.110201) from day 46 post-Den.
600 Tumours were allowed to develop before mice were humanely killed at day 270 post-Den. For the poorly-
601 metastatic model of lung adenocarcinoma, 8-10 week old KM (*KRas*$^{G12D/+}$ [52]; *Rosa26*$^{lsl\text{-}Myc/lsl\text{-}Myc}$ [18]) mice were
602 induced with 1x10^{7} pfu Adeno-*Cre* recombinant adenovirus (University of Iowa gene therapy core facility), as
603 described previously. Induced KM mice and un-induced litter mates were humanely killed after 6 weeks when
604 mice displayed no clinical signs but had macroscopic lesions[18], and tissues harvested for analysis. For highly-
605 metastatic and poorly-metastatic models of PDAC and their controls, WT, *Kras*^{G12D}; *Pdx1*^{Cre} (KC), *Kras*^{G12D};
606 *Trp53*$^{fl/+}$; *Pdx1*^{Cre} (KP^{fl}C) and *Kras*^{G12D}; *Trp53*$^{R172H/+}$; *Pdx1*^{Cre} (KPC) were used[19, 53]. Mice were monitored at least
607 3 times weekly. KP^{fl}C and KPC mice were humanely killed upon detection of a palpable primary tumour, prior
608 to the development of macroscopic metastasis, and age matched WT controls and KC mice were humanely
609 killed at the same time.

610 **Tissue preparation for flow cytometry**

611 Blood was collected in 2mM EDTA (ThermoFisher) coated syringes by cardiac puncture under terminal
612 anaesthesia (sodium pentobarbital, i.p.) and red blood cells (RBC) were lysed. BM cells were harvested from
613 the femur by flushing the bone through a 70µm filter with RPMI/5% (v/v) FBS/2mM EDTA. Lungs were excised
614 and then minced with scissors before incubation in RPMI (ThermoFisher) with 10% foetal bovine serum (FBS,
615 ThermoFisher) at 37°C for 20 minutes with agitation. Post-incubation, lungs were mashed through a 70µm
616 filter. Spleens were excised and mashed through a 70µm filter. Livers and liver tumours were excised and
617 then minced with scissors before incubation in RPMI/10% (v/v) FBS/2mM EDTA/1.2mg/mL Collagenase D
618 (Roche)/1mg/mL DNase I (Roche) at 37°C for 20 minutes with agitation. Post-incubation livers were mashed
619 through a 70µm followed by a 40µm filter. A section of small intestine was excised, flushed with RPMI/2%
620 (v/v) FBS and minced with scissors before incubation in RPMI/75µg/mL DNase I/2mg/mL Collagenase D at
621 37°C for 30 minutes with agitation. Post-incubation, small intestines were mashed through a 70µm filter
622 followed by a 40µm filter. Pancreatic tumours were excised and then minced with scissors before incubation
623 in RPMI/75µg/mL DNase I/2mg/mL Collagenase D at 37°C for 30 minutes with agitation. Post-incubation,
624 pancreatic tumours were mashed through a 70µm filter followed by a 40µm filter. Intestinal tumours were
625 excised and then minced with scissors before incubation in RPMI/75µg/mL DNase I/2mg/mL Collagenase D
626 at 37°C for 30 minutes with agitation. Post-incubation intestinal tumours were mashed through a 70µm filter
627 followed by a 40µm filter.

628

629 **Extracellular protein staining for flow cytometry analysis**

630 Single cell suspensions were stained with Live/Dead stain (LIVE/DEAD Fixable Near-IR or Yellow, Biolegend)
631 and Fc-Receptor block was performed (using clone 93, Biolegend). Cell suspensions were incubated with
632 directly conjugated fluorescent antibodies in PBS/1% (w/v) BSA (Merck)/0.05% (v/v) Sodium Azide
633 (GBiosciences) (PBA) buffer at 4°C for 30 minutes. Biotinylated antibodies were labelled with fluorescently
634 conjugated Streptavidin in PBA at 4°C for 30 minutes.

635

636

637 **Intracellular protein staining for flow cytometry analysis**

638 Following extracellular protein staining, cells were fixed and permeabilized (Invitrogen) prior to staining with
639 directly conjugated fluorescent antibodies at 4°C for 30-60 minutes. For Ki-67 staining, after extracellular
640 staining cells were fixed with 2% PFA for 10 minutes at room temperature and washed with PBS. Cells were
641 then re-suspended in fluorescently-conjugated Ki-67 antibody in PBS for 25 minutes at room temperature.
642 Cells were washed with PBS prior to analysis.

643

644 **Flow cytometry acquisition and analysis**

645 Count beads (CountBright, Life Technologies) were used to determine cell numbers. Compensation was
646 performed using single stained beads (Ultracomp eBeads, ThermoFisher). Fluorescence minus one (FMO)
647 controls were used to determine accurate gating. Acquisition was performed on a BDFortessa using FacsDiva
648 software (BD Biosciences) and data analysed using FlowJo software (BD).

649

650 **Tissue preparation for Fluorescence Activated Cell Sorting (FACS)**

651 For FACS of neutrophils for RNA-Seq analysis, PB, BM, SP and LV was collected as for flow cytometry. For *ex*
652 *vivo* culture and adoptive transfer of neutrophils post-sorting, BM cells were harvested from the femur, tibia,
653 radius and ulna dependent on the cell numbers required and collected into PBS/5% (v/v) FBS/1% (v/v)
654 Penicillin/Streptomycin (ThermoFisher). All subsequent processing was undertaken in a biological safety level
655 2 tissue culture hood with sterile reagents. Bones were washed in 70% EtOH and flushed as for flow
656 cytometry with RPMI/5% (v/v) FBS/2mM EDTA/1% (v/v) Penicillin/Streptomycin. BM cells were enriched for
657 neutrophils using a mouse neutrophil negative enrichment kit (Biolegend).

658

659 **Extracellular protein staining for FACS**

660 For RNA-Seq analysis, single cell suspensions were stained as for flow cytometry, however Live/Dead stain
661 was not performed and instead 4'-6'-diamidino-2-phenylindole (DAPI, ThermoFisher) was added
662 immediately prior to sorting for live/dead detection. For *ex vivo* culture and adoptive transfer of neutrophils
663 post-sorting, single cell suspensions were stained as for flow cytometry but in sterile PBS/1% (v/v) FBS/1mM

664 EDTA. For sorting, cells were re-suspended in PBS/1% (v/v) FBS/1% (v/v) Pen/Strep/5mM EDTA/25mM HEPES
665 (ThermoFisher).
666
667 **FACS acquisition**
668 Acquisition was performed on a BD FACSAria sorter situated within a biological safety level 2 enclosure at
669 4°C using a 100µm nozzle at the slowest acquisition speed and at a flow rate of approximately 2,000
670 events/second. For RNA-Seq analysis, populations were sorted into 15mL Falcon tubes coated with PBS/10%
671 (v/v) FBS and containing PBA buffer. For *ex* vivo culture and adoptive transfer experiments, neutrophil
672 populations were sorted into 15mL Falcon tubes coated with RPMI/10% (v/v FBS) and containing RPMI/20%
673 (v/v) FBS/5mM EDTA/25mM HEPES/1% (v/v) Pen/Strep.
674
675 **Antibodies and reagents for flow cytometry/FACS**
676 The following antibodies were used: CD45 (clone 30-F11), CD11b (clone M1/70), Ly6G (clone 1A8), CD3e
677 (clone 145-2C11), CD19 (clone 6D5), Nkp46 (clone 29A1.4), Ter119 (clone TER119) ICAM-1 (clone YN1/1.7.4),
678 CD115 (clone AFS98), CD117 (clone 2B8), Sca-1 (clone D7), CCR6 (clone 29-2L17), CD48 (clone HM48-1), Ki-
679 67 (clone 16A8), CD16/32 (clone 93), CD18 (clone M18/2), CXCR4 (clone L276F12), CXCR2 (clone SA045E1),
680 Streptavidin (all Biolegend), Ly6B.2 (clone 7/4, Bio-Rad), CD133 (clone 13A4, eBioscience), CD49d (clone R1-
681 2, ThermoFisher), CD101 (clone Moushi101, ThermoFisher), Siglec-F (clone E50-2440, BD Biosciences), CCR1
682 (clone 643854, Bio-Techne).
683
684 **Cell trace staining**
685 Sorted BM Ly6G^{Int} and Ly6G^{Hi} neutrophil populations, and CD3^{+} T cells enriched from the spleen of naïve
686 mice, were incubated for 15 minutes at 37°C with CellTrace CFDA-SE (ThermoFisher), CellTrace Yellow
687 (ThermoFisher) or CellTrace Red (ThermoFisher) diluted in sterile PBS. Cells were washed in
688
689 **CSF-3-induced acute haematopoietic stress**

690 Female C57BL/6 mice received a single dose of mouse recombinant CSF-3 (StemCell Technologies) at
691 0.25mg/kg in sterile PBS, or sterile PBS alone for control, by i.p. injection for the specified time-period at
692 which point the mice were sacrificed.
693
694 **LPS-induced acute systemic inflammation**
695 Mice received a single dose of LPS 0111:B4 from *Escheria coli* (Merck) at 1mg/kg in sterile PBS, or sterile PBS
696 alone for control, by i.p. injection for the specified time-period at which point the mice were sacrificed.
697
698 **EdU incorporation assay**
699 Female C57BL/6 mice received a single dose of the thymidine analogue EdU (ThermoFisher) at 50mg/kg in
700 sterile PBS by i.p. injection for the specified time-period at which point the mice were sacrificed. Cells were
701 isolated and labelled with directly conjugated fluorescent antibodies as for flow cytometry. After labelling,
702 cells were fixed and stained for EdU following the manufacturer's instruction and analysed by flow cytometry.
703
704 **Neutrophil adoptive transfer and lung extraction**
705 $Ly6G^{Int}$ and $Ly6G^{Hi}$ neutrophil populations were FACS sorted from the BM of CSF-3 challenged mice and cell
706 trace stained, as previously described. Post-cell trace staining, $1.5x10^6$ cells from each neutrophil population
707 was mixed into a final volume of 100µL and intravenously (i.v.) injected into the tail vein of PBS control or
708 LPS challenged mice. Mice were sacrificed and blood was collected as for flow cytometry. The right lung lobe
709 was tied off, a small incision made to the trachea and a customized blunted 22G needle inserted. The left
710 lung was inflated with 0.6mL PBS/2% (w/v) low melting point agarose (Merck) in PBS. The right lung lobe was
711 excised for processing by flow cytometry. The inflated left lobe was excised and fixed in PBS/4% (v/v)
712 formaldehyde (VWR) for 2 hours at 4°C.
713
714 **Fixed precision cut lung slices (PCLS)**
715 Fixed lungs were sliced into 300µm thick sections on a vibrating microtome (Campden Ltd). Slices were
716 stained with Hamster anti-CD31 ab (2H8, Abcam) in PBS/1% (w/v) bovine serum albumin (BSA, Sigma)/10%

717 (v/v) normal goat serum (NGS, Sigma)/0.001% (v/v) sodium-azide (VWR). Hamster-IgG (ThermoFisher) were
718 used to control for unspecific staining. Anti-Hamster Cy3 (Jackson) was used as a secondary antibody and
719 DAPI to stain nuclei.
720
721 **Confocal imaging**
722 PCLS prepared and stained as described above were imaged on a Zeiss LSM880 confocal microscope,
723 processed in Zeiss Software before quantification and analysis using Imaris software (Bitplane, Oxford
724 Instruments).
725
726 **Bulk RNA isolation, sequencing and normalization**
727 All mice used for RNA isolation were humanely killed within the same period in the morning (between 07.00-
728 08.30) to minimise circadian-induced gene expression changes between samples. RNA was isolated from
729 Ly6G^{Int} , Ly6G^{Hi} or Ly6G^{+} neutrophil populations that had been FACS sorted from the BM, spleen and
730 peripheral blood. Biological replicates for PBS and LPS bulk Ly6G^{+} neutrophil RNA-Seq are as follows: PBS:
731 peripheral blood Ly6G^{Hi} n=4 mice; BM Ly6G^{Int} n=4 mice; BM Ly6G^{Hi} n=4 mice; spleen Ly6G^{Int} n=6 mice; spleen
732 Ly6G^{Hi} n=7 mice; liver Ly6G^{+} n=7 mice. LPS: peripheral blood Ly6G^{Int} n=4 mice; peripheral blood Ly6G^{Hi} n=4
733 mice; BM Ly6G^{Int} n=3 mice; BM Ly6G^{Hi} n=3 mice; spleen Ly6G^{Int} n=4 mice; spleen Ly6G^{Hi} n=4 mice; liver Ly6G^{+}
734 n=4 mice. Biological replicates for PDAC model bulk Ly6G^{+} neutrophil RNA-Seq are as follows: BM: WT Ly6G^{Int}
735 n=10 mice; KP^{fl}C Ly6G^{Int} n=5 mice; KPC Ly6G^{Int} n=5 mice; KPC Ly6G^{Hi} n=5 mice. Spleen: WT Ly6G^{Int} n=8 mice;
736 KP^{fl}C Ly6G^{Int} n=4 mice; KPC Ly6G^{Int} n=5 mice.
737 RNA was extracted from sorted populations using an RNeasy Micro Kit (Qiagen). RNA quality was
738 evaluated using an Agilent Bioanalyser using RNA Pico chips. Libraries for cluster generation and DNA
739 sequencing were prepared using a TaKaRa SMARTer Stranded Total RNA-Seq – Pico Input Mammalian kit
740 v2.0 as per the manufacturer's instructions. Quality and quantity of the DNA libraries was assessed on an
741 Agilent 2200 Tapestation (D1000 screentape) and Qubit (Thermo Fisher Scientific) respectively. The libraries
742 were run on the Illumina Next Seq 500 using the High Output 75 cycles kit (2x36 cycles, paired end reads,
743 dual index). Illumina data were demultiplexed using bcl2fastq version 2.19.0.216, then adaptor sequences

744 were removed using Cutadapt version 0.6.4. Next, quality checks on fastq files were performed using fastqc
745 version 0.11.8. Paired-end reads were then aligned to the mouse genome version GRCh38.95 using HISAT2
746 version 2.1.0 with the –known-splicesite-infile and –rna-strandness options. Expression levels were
747 determined using HTseq version 0.11.2 with the -s=reverse, --mode=intersection-nonempty and –type=exon
748 options, then statistically analysed using R version 3.5.1. Differential gene expression analysis based on the
749 negative binomial distribution was performed using DESeq2 version 1.22.2[54].
750

751 **Identification of reliably expressed genes and DEGs from RNA-Seq**

752 From normalized data, genes with reliable expression were identified as those with ≥ 2 reads/million in at
753 least half of the replicates per neutrophil population. Genes not matching these conditions were excluded.
754 DEGs were identified as those with a fold change ≥ 1.5 and P-value ≤ 0.05 between compared populations.
755

756 **Bulk proteomic analysis.**

757 Ly6G^{Int} and Ly6G^{Hi} neutrophil populations were sorted from the peripheral blood and BM of CSF-3 (i.p. 0.25
758 mg/kg, 24 hours) administered mice. BM Ly6G^{Int} n=3, and peripheral blood and BM Ly6G^{Hi} n=3 replicates.
759 Each replicate was composed of FACS isolated Ly6G^{Int} and Ly6G^{Hi} neutrophils pooled from n=4 mice. Sorted
760 neutrophil populations were pelleted, snap frozen in liquid nitrogen and stored at -70°C. Sorted neutrophil
761 populations from 4 mice per replica were thawed and pooled. Samples were lysed by boiling with sodium
762 dodecyl sulfate (SDS), sonicated and centrifuged for debris removal. Proteins obtained in the supernatants
763 were precipitated in two steps using 24% and 10% solution of trichloroacetic acid. In both steps, pellets were
764 incubated at 4°C for 10 min and centrifuged at 18,000 g for 5 min. Supernatants were carefully aspirated and
765 pellets were washed with water until the supernatant reached neutral pH. Pellets were reconstituted in…
766 and digested, first using Endoproteinase Lys-C (ratio 1:33 enzyme:lysate, Alpha Laboratories) for 1 h at room
767 temperature, then with trypsin (ratio 1:33 enzyme:lysate, Promega) overnight at 35°C. *Off-line HPLC*
768 *fractionation:* TMT-labelled peptides were fractionated using high pH reverse phase chromatography on a
769 C18 column (150 × 2.1 mm i.d. - Kinetex EVO (5 µm, 100 Å)) on a HPLC system (Agilent, LC 1260 Infinity II,
770 Agilent). A two-step gradient was applied, from 1–28% B in 42 min, then from 28–46% B in 13 min. The

771 column eluate was collected into 9 fractions subsequently submitted to MS analysis. *UHPLC-MS/MS analysis:*
772 Fractionated tryptic digests were separated by nanoscale C18 reverse-phase liquid chromatography using an
773 EASY-nLC II 1200 (Thermo Fisher Scientific) coupled to an Orbitrap Fusion Lumos mass spectrometer (Thermo
774 Fisher Scientific). Samples were loaded into a 50 cm fused silica emitter (New Objective) packed in-house
775 with ReproSil-Pur C18-AQ, 1.9 µm resin (Dr Maisch GmbH). The emitter was kept at 50 °C by means of a
776 column oven (Sonation) integrated into the nanoelectrospray ion source (Thermo Fisher Scientific). Elution
777 was carried out at a flow rate of 300 nl/min using a binary gradient with buffer A (2% acetonitrile) and B
778 (80% acetonitrile), both containing 0.1% formic acid. Peptides from each fraction were eluted at using three
779 different binary gradients optimised for different set of fractions as described previously[55]. An Active
780 Background Ion Reduction Device (ESI Source Solutions) was used to decrease air contaminants signal level.
781 Data were acquired using Xcalibur software (Thermo Fisher Scientific) on an Orbitrap Fusion Lumos mass
782 spectrometer (Thermo Fisher Scientific). The mass spectrometer was operated in positive ion mode and used
783 in data-dependent acquisition (DDA). A full scan was acquired over mass range of 350-1400 m/z, with 60,000
784 resolution at 200 m/z, for a maximum injection time of 20 ms and with a target value of 9e5 ions with
785 "monoisotopic precursor selection" set to "Peptide" mode. Higher energy collisional dissociation
786 fragmentation was performed on the 15 most intense ions, for a maximum injection time of 150 ms, or a
787 target value of 500,000 ions. Peptide fragments were analysed in the Orbitrap at 50,000 resolution.
788 *Proteomic Data analysis:* The MS Raw data were processed with MaxQuant software[56] version 1.6.3.3 and
789 searched with Andromeda search engine[57], querying UniProt[58] *Mus musculus* (12/08/2018; 25,198 entries).
790 First and main searches were carried out with precursor mass tolerances of 20 ppm and 4.5 ppm,
791 respectively, and MS/MS tolerance of 20 ppm. The minimum peptide length was set to six amino acids and
792 specificity for trypsin cleavage was required, allowing up to two missed cleavage sites. MaxQuant was set to
793 quantify on "Reporter ion MS2", and TMT10plex was chose as Isobaric label. Interference between TMT
794 channels were corrected by MaxQuant using the correction factors provided by the manufacturer. The "Filter
795 by PIF" option was activated and a "Reporter ion tolerance" of 0.003 Da was used. Methionine oxidation and
796 N-terminal acetylation were specified as variable modifications, and Cysteine carbamidomethylation was set
797 as fixed modification. The peptide and protein false discovery rate (FDR) was set to 1 %. MaxQuant output

798 was further processed and analysed using Perseus software version 1.6.2.3. Protein quantification was done
799 using the ProteinGroups.txt file, Reverse and Potential Contaminant proteins were removed, and at least one
800 uniquely assigned peptide and a minimum ratio count of 2 were required for a protein to be quantified. To
801 identify regulated proteins, ANOVA "Multiple sample test" in Perseus was used with a truncation threshold
802 value of 0.001 (Permutation based FDR) and S0=0. The test was applied to the 3 groups considered. For data
803 visualisation, proteins that passed the ANOVA test were z-score normalised. Hierarchical clustering analysis
804 was performed using "Euclidian distance" for both rows and columns.
805
806 **Splenic T-cell enrichment and *ex vivo* suppression assays**
807 T cells were enriched from single cell suspensions of splenocytes isolated from naïve C57BL/6 mice as for
808 flow cytometry using a mouse CD3 T cell negative selection kit (Biolegend). Enriched $CD3^+$ T cells were cell
809 trace stained and cultured at $1x10^6$ cells/mL and stimulated with mouse T-activator anti-CD3/CD28
810 Dynabeads (ThermoFisher) at a 1:1 ratio. T cells were incubated with $Ly6G^{Int}$ or $Ly6G^{Hi}$ neutrophil populations
811 sorted from the BM of naïve or CSF-3 challenged mice at varying ratios for 48 hours at 37°C, 5% CO_2. Post-
812 incubation cells were stained with a live/dead stain, labelled with anti-CD4 and anti-CD8 fluorescently
813 conjugated antibodies and analysed by flow cytometry.
814
815 **Neutrophil *ex vivo* culture**
816 $Ly6G^{Int}$ and $Ly6G^{Hi}$ neutrophil populations were sorted from the BM of naïve C57BL/6 mice. $1.75x10^3$ cells
817 were loaded into individual well of a 96 well v-bottom plate in RPMI/5% (v/v) FBS/2mM EDTA/1% (v/v)
818 Penicillin/Streptomycin/1% (v/v) L-Glutamine (ThermoFisher)/0.1% (v/v) β-Mercaptoethanol
819 (ThermoFisher). Cells were incubated for the required time at 37°C, 5% CO_2. Post-incubation total cell
820 numbers were manually counted using a haemocytometer (Hausser Scientific) and stained for flow cytometry
821 analysis.
822
823
824

825 **Data availability**

826 The accession code for RNA-Seq data is pending and data are currently available by contacting the
827 corresponding author. The mass spectrometry proteomics data have been deposited to the
828 ProteomeXchange Consortium via the PRIDE partner repository[59] with the dataset identifier PXD026708. All
829 other data are available by contacting the corresponding author.

830

831 **Quantification and statistical analysis**

832 Statistical analyses were performed using GraphPad Prism software (v8.0 GraphPad software, USA).
833 Statistical tests used are as specified in figure legends.

834

835 **Author Contributions**

836 JBGM and LMC conceived the study. JBGM, AJM, TJ, RJ, XLR, JS, WC, AH, KG, XC, and SL performed
837 experiments. JBGM, AJM, XLR, WC, AH, KG, FF, SL, JV and LMC analysed and interpreted data. AJM, TJ, RJ,
838 XLR, GJG, DJM, CWS, JCN, TGB, DJM, SZ, JM, OJS advised on and provided mouse cancer models. JBGM and
839 LMC wrote the manuscript. All authors reviewed and edited the manuscript.

840

841 **Acknowledgements**

842 **General:** We would like to thank the core services and advanced technologies at the National Heart and Lung
843 Institute and the CRUK Beatson Institute with particular thanks to the Biological Services Unit, Molecular
844 Services, Bioinformatics and the Beatson Advanced Imaging Resource with particular thanks to Tom Gilbey
845 for cell sorting. We would like to thank the members of the Leukocyte Dynamics Group and Catherine
846 Winchester for critical reading of the manuscript. We would also like to thank Sara Rankin and Clare Lloyd
847 for helpful discussions during the project.

848 **Funding:** JBGM was supported by an Imperial College London NHLI Foundation studentship, MRC grant
849 (MR/M01245X/1) and CRUK core funding (A17196 and A31287). LMC (CRUK A23983), OJS (CRUK A21339),
850 JCN (CRUK A18277), JM (CRUK A29996) and SZ (CRUK A29800) were supported by CRUK core funding at

Cancer Research UK Beatson Institute. TGB was funded by Wellcome (WT107492Z) and the CRUK HUNTER Accelerator Award (CRUK A26813).

Conflict of interest

The authors are declaring no competing financial interests in the relation to the work described.

References

1. Ng, L.G., Ostuni, R. & Hidalgo, A. Heterogeneity of neutrophils. *Nat Rev Immunol* **19**, 255-265 (2019).

2. Pfirschke, C. *et al.* Tumor-Promoting Ly-6G(+) SiglecF(high) Cells Are Mature and Long-Lived Neutrophils. *Cell Rep* **32**, 108164 (2020).

3. Ballesteros, I. *et al.* Co-option of Neutrophil Fates by Tissue Environments. *Cell* (2020).

4. Sagiv, J.Y. *et al.* Phenotypic diversity and plasticity in circulating neutrophil subpopulations in cancer. *Cell Rep* **10**, 562-573 (2015).

5. Deniset, J.F., Surewaard, B.G., Lee, W.Y. & Kubes, P. Splenic Ly6G(high) mature and Ly6G(int) immature neutrophils contribute to eradication of S. pneumoniae. *J Exp Med* **214**, 1333-1350 (2017).

6. Juzenaite, G. *et al.* Lung Marginated and Splenic Murine Resident Neutrophils Constitute Pioneers in Tissue-Defense During Systemic E. coli Challenge. *Front Immunol* **12**, 597595 (2021).

7. Faurschou, M. & Borregaard, N. Neutrophil granules and secretory vesicles in inflammation. *Microbes Infect* **5**, 1317-1327 (2003).

8. Grieshaber-Bouyer, R. *et al.* The neutrotime transcriptional signature defines a single continuum of neutrophils across biological compartments. *Nat Commun* **12**, 2856 (2021).

9. Khoyratty, T.E. *et al.* Distinct transcription factor networks control neutrophil-driven inflammation. *Nature Immunology* (2021).

10. Evrard, M. *et al.* Developmental Analysis of Bone Marrow Neutrophils Reveals Populations Specialized in Expansion, Trafficking, and Effector Functions. *Immunity* **48**, 364-379 e368 (2018).

11. Mare, T.A. *et al.* The diagnostic and prognostic significance of monitoring blood levels of immature neutrophils in patients with systemic inflammation. *Crit Care* **19**, 57 (2015).

12. Carissimo, G. *et al.* Whole blood immunophenotyping uncovers immature neutrophil-to-VD2 T-cell ratio as an early marker for severe COVID-19. *Nat Commun* **11**, 5243 (2020).

13. Lukasova, E. *et al.* Granulocyte maturation determines ability to release chromatin NETs and loss of DNA damage response; these properties are absent in immature AML granulocytes. *Biochim Biophys Acta* **1833**, 767-779 (2013).

898 14. Rice, C.M. *et al.* Tumour-elicited neutrophils engage mitochondrial metabolism to circumvent
899 nutrient limitations and maintain immune suppression. *Nat Commun* **9**, 5099 (2018).
900
901 15. Mackey, J.B.G., Coffelt, S.B. & Carlin, L.M. Neutrophil Maturity in Cancer. *Front Immunol* **10**, 1912
902 (2019).
903
904 16. Xie, X. *et al.* Single-cell transcriptome profiling reveals neutrophil heterogeneity in homeostasis and
905 infection. *Nat Immunol* **21**, 1119-1133 (2020).
906
907 17. Jackstadt, R. *et al.* Epithelial NOTCH Signaling Rewires the Tumor Microenvironment of Colorectal
908 Cancer to Drive Poor-Prognosis Subtypes and Metastasis. *Cancer Cell* **36**, 319-336 e317 (2019).
909
910 18. Kruspig, B. *et al.* The ERBB network facilitates KRAS-driven lung tumorigenesis. *Sci Transl Med* **10**
911 (2018).
912
913 19. Morton, J.P. *et al.* Mutant p53 drives metastasis and overcomes growth arrest/senescence in
914 pancreatic cancer. *Proc Natl Acad Sci U S A* **107**, 246-251 (2010).
915
916 20. Klausen, P., Bjerregaard, M.D., Borregaard, N. & Cowland, J.B. End-stage differentiation of
917 neutrophil granulocytes in vivo is accompanied by up-regulation of p27kip1 and down-regulation of
918 CDK2, CDK4, and CDK6. *J Leukoc Biol* **75**, 569-578 (2004).
919
920 21. Porse, B.T. *et al.* E2F repression by C/EBPalpha is required for adipogenesis and granulopoiesis in
921 vivo. *Cell* **107**, 247-258 (2001).
922
923 22. Pedersen, C.C. *et al.* Changes in Gene Expression during G-CSF-Induced Emergency Granulopoiesis
924 in Humans. *J Immunol* **197**, 1989-1999 (2016).
925
926 23. Ulich, T.R., del Castillo, J. & Souza, L. Kinetics and mechanisms of recombinant human granulocyte-
927 colony stimulating factor-induced neutrophilia. *Am J Pathol* **133**, 630-638 (1988).
928
929 24. Delano, M.J. *et al.* Neutrophil mobilization from the bone marrow during polymicrobial sepsis is
930 dependent on CXCL12 signaling. *J Immunol* **187**, 911-918 (2011).
931
932 25. Hasenberg, A. *et al.* Catchup: a mouse model for imaging-based tracking and modulation of
933 neutrophil granulocytes. *Nat Methods* **12**, 445-452 (2015).
934
935 26. Satake, S. *et al.* C/EBPbeta is involved in the amplification of early granulocyte precursors during
936 candidemia-induced "emergency" granulopoiesis. *J Immunol* **189**, 4546-4555 (2012).
937
938 27. Kim, M.H. *et al.* A late-lineage murine neutrophil precursor population exhibits dynamic changes
939 during demand-adapted granulopoiesis. *Sci Rep* **7**, 39804 (2017).
940
941 28. Coffelt, S.B. *et al.* IL-17-producing gammadelta T cells and neutrophils conspire to promote breast
942 cancer metastasis. *Nature* **522**, 345-348 (2015).
943
944 29. Hager, M., Cowland, J.B. & Borregaard, N. Neutrophil granules in health and disease. *J Intern Med*
945 **268**, 25-34 (2010).
946
947 30. Williams, A.E. & Chambers, R.C. The mercurial nature of neutrophils: still an enigma in ARDS? *Am J*
948 *Physiol Lung Cell Mol Physiol* **306**, L217-230 (2014).
949

31. Park, I. *et al.* Neutrophils disturb pulmonary microcirculation in sepsis-induced acute lung injury. *Eur Respir J* **53** (2019).

32. Domscheit, H., Hegeman, M.A., Carvalho, N. & Spieth, P.M. Molecular Dynamics of Lipopolysaccharide-Induced Lung Injury in Rodents. *Front Physiol* **11**, 36 (2020).

33. Zhu, Y.P. *et al.* Identification of an Early Unipotent Neutrophil Progenitor with Pro-tumoral Activity in Mouse and Human Bone Marrow. *Cell Rep* **24**, 2329-2341 e2328 (2018).

34. Furze, R.C. & Rankin, S.M. Neutrophil mobilization and clearance in the bone marrow. *Immunology* **125**, 281-288 (2008).

35. Summers, C. *et al.* Neutrophil kinetics in health and disease. *Trends Immunol* **31**, 318-324 (2010).

36. Nemeth, T., Sperandio, M. & Mocsai, A. Neutrophils as emerging therapeutic targets. *Nat Rev Drug Discov* **19**, 253-275 (2020).

37. Granot, Z. Neutrophils as a Therapeutic Target in Cancer. *Front Immunol* **10**, 1710 (2019).

38. Hsu, B.E. *et al.* Immature Low-Density Neutrophils Exhibit Metabolic Flexibility that Facilitates Breast Cancer Liver Metastasis. *Cell Rep* **27**, 3902-3915 e3906 (2019).

39. Kusmartsev, S., Nagaraj, S. & Gabrilovich, D.I. Tumor-associated CD8+ T cell tolerance induced by bone marrow-derived immature myeloid cells. *J Immunol* **175**, 4583-4592 (2005).

40. Puga, I. *et al.* B cell-helper neutrophils stimulate the diversification and production of immunoglobulin in the marginal zone of the spleen. *Nat Immunol* **13**, 170-180 (2011).

41. Massberg, S. *et al.* Immunosurveillance by hematopoietic progenitor cells trafficking through blood, lymph, and peripheral tissues. *Cell* **131**, 994-1008 (2007).

42. Miwa, Y. *et al.* Up-regulated expression of CXCL12 in human spleens with extramedullary haematopoiesis. *Pathology* **45**, 408-416 (2013).

43. Oda, A. *et al.* Niche-induced extramedullary hematopoiesis in the spleen is regulated by the transcription factor Tlx1. *Sci Rep* **8**, 8308 (2018).

44. Wu, C. *et al.* Spleen mediates a distinct hematopoietic progenitor response supporting tumor-promoting myelopoiesis. *J Clin Invest* **128**, 3425-3438 (2018).

45. Jhunjhunwala, S. *et al.* Frontline Science: Splenic progenitors aid in maintaining high neutrophil numbers at sites of sterile chronic inflammation. *J Leukoc Biol* **100**, 253-260 (2016).

46. Alshetaiwi, H. *et al.* Defining the emergence of myeloid-derived suppressor cells in breast cancer using single-cell transcriptomics. *Sci Immunol* **5** (2020).

47. Wu, C., Hua, Q. & Zheng, L. Generation of Myeloid Cells in Cancer: The Spleen Matters. *Front Immunol* **11**, 1126 (2020).

48. Stoth, M. *et al.* Splenectomy reduces lung metastases and tumoral and metastatic niche inflammation. *Int J Cancer* **145**, 2509-2520 (2019).

1002 49. Lambert, A.W., Pattabiraman, D.R. & Weinberg, R.A. Emerging Biological Principles of Metastasis.
1003 *Cell* **168**, 670-691 (2017).
1004
1005 50. Bao, Y. *et al.* Extramedullary hematopoiesis secondary to malignant solid tumors: a case report and
1006 literature review. *Cancer Manag Res* **10**, 1461-1470 (2018).
1007
1008 51. Kim, M.H. *et al.* Neutrophil survival and c-kit(+)-progenitor proliferation in Staphylococcus aureus-
1009 infected skin wounds promote resolution. *Blood* **117**, 3343-3352 (2011).
1010
1011 52. Jackson, E.L. *et al.* Analysis of lung tumor initiation and progression using conditional expression of
1012 oncogenic K-ras. *Genes Dev* **15**, 3243-3248 (2001).
1013
1014 53. Hingorani, S.R. *et al.* Trp53R172H and KrasG12D cooperate to promote chromosomal instability and
1015 widely metastatic pancreatic ductal adenocarcinoma in mice. *Cancer Cell* **7**, 469-483 (2005).
1016
1017 54. Anders, S. & Huber, W. Differential expression analysis for sequence count data. *Genome Biol* **11**,
1018 R106 (2010).
1019
1020 55. van der Reest, J., Lilla, S., Zheng, L., Zanivan, S. & Gottlieb, E. Proteome-wide analysis of cysteine
1021 oxidation reveals metabolic sensitivity to redox stress. *Nat Commun* **9**, 1581 (2018).
1022
1023 56. Cox, J. & Mann, M. MaxQuant enables high peptide identification rates, individualized p.p.b.-range
1024 mass accuracies and proteome-wide protein quantification. *Nat Biotechnol* **26**, 1367-1372 (2008).
1025
1026 57. Cox, J. *et al.* Andromeda: a peptide search engine integrated into the MaxQuant environment. *J*
1027 *Proteome Res* **10**, 1794-1805 (2011).
1028
1029 58. UniProt, C. The Universal Protein Resource (UniProt) in 2010. *Nucleic Acids Res* **38**, D142-148
1030 (2010).
1031
1032 59. Perez-Riverol, Y. *et al.* The PRIDE database and related tools and resources in 2019: improving
1033 support for quantification data. *Nucleic Acids Res* **47**, D442-D450 (2019).
1034
1035